Identification of USP7 as an essential component to maintain integrity and function of non-canonical PRC1.1 in leukemia

Henny Maat[1], Jennifer Jaques[1], Aida Rodríguez López[1], Shanna M. Hogeling[1], Marcel P. de Vries[2,3], Chantal Gravesteijn[1], Annet Z. Brouwers-Vos[1], Gerwin Huls[1], Edo Vellenga[1], Vincent van den Boom[1] and Jan Jacob Schuringa[1,*].

[1]Department of Experimental Hematology, Cancer Research Center Groningen, University Medical Center Groningen, University of Groningen, Hanzeplein 1, 9713 GZ Groningen, The Netherlands;

[2]Department of Pharmacy, Interfaculty Mass Spectrometry Center, University of Groningen, A. Deusinglaan 1, 9713 AV Groningen, The Netherlands;

[3]Department of Pediatrics, Center for Liver, Digestive, and Metabolic Diseases, University Medical Center Groningen, University of Groningen, Hanzeplein 1, 9713 GZ Groningen, The Netherlands

[*]Correspondence: j.j.schuringa@umcg.nl. Department of Experimental Hematology, Medical Center Groningen, University of Groningen, Hanzeplein 1, DA13, 9713 GZ Groningen, The Netherlands.

ABSTRACT

Polycomb proteins are essential epigenetic regulators of gene transcription. KDM2B, the chromatin-binding moiety of non-canonical PRC1.1, is critically important for human leukemias. Here, we investigated the complete interactome of KDM2B in human leukemic cells and identified that the deubiquitinase USP7 is an essential component of PRC1.1 and required for its stability and function. USP7 inhibition results in disassembly of the PRC1.1 complex and consequently loss of binding to its target loci. PRC1.1 can be associated with active loci and loss of PRC1.1 binding coincided with loss of H2AK119ub, reduced H3K27ac levels and reduced gene transcription, whereas H3K4me3 levels remained unaffected. Survival was reduced in (primary) acute myeloid leukemia cells in both cycling as well as quiescent populations upon USP7 inhibition, also independent of the USP7-MDM2-p53 axis. Finally, we evaluated the efficacy of USP7 inhibition *in vivo* and find that progression of MLL-AF9-induced leukemia is delayed, although in a niche-dependent manner.

KEYWORDS

chromatin occupancy / deubiquitinase / leukemia / non-canonical PRC1.1 / USP7

36 **INTRODUCTION**

37 Regulation of gene transcription is carefully coordinated to control stem cell self-renewal and
38 differentiation. Polycomb group (PcG) proteins are important epigenetic regulators and critically
39 involved in controlling gene transcription by mediating post-translational modifications of histone
40 proteins and chromatin remodeling [1-3]. Genome-wide analyses of Polycomb target genes revealed
41 the occupancy of PcG proteins at promoters of genes regulating cell fate, highlighting their
42 importance for proper lineage specification [4-6]. Yet, how PcG proteins are recruited, recognize
43 their target genes and regulate gene expression still remains poorly understood. Understanding
44 these processes is important since deregulation of PcG proteins frequently contributes to cancer and
45 hematopoietic malignancies, like leukemia [7-9].

46

47 PcG proteins form multi-protein chromatin modifying complexes of which Polycomb Repressive
48 Complex 1 (PRC1) and 2 (PRC2) are best characterized [10]. PRC2, by means of EZH1/EZH2, catalyzes
49 the trimethylation of histone H3 on lysine 27 (H3K27me3) which can be recognized by the
50 chromodomain protein (CBX) of the canonical PRC1 complex [11-13]. PRC1 monoubiquitinates
51 histone H2A on lysine 119 (H2AK119ub) via either one of the two E3 ligases RING1A/1B [14,15].
52 Proteome analysis has identified the composition of six major PRC1 complexes that all contain
53 RING1A or RING1B and distinguished by the presence of one of the six PCGF proteins (PCGF1-6)
54 [16,17]. Canonical PRC1 complexes contain either PCGF2 or PCGF4 and one of the CBX paralogs
55 (CBX2/4/6/7/8), PHC (1/2/3) and SCML1/SCML2/SCMH1 subunits. Non-canonical PRC1 complexes
56 lack a CBX subunit and instead contain RYBP or YAF2 which all three compete for the same binding
57 site of RING1B [16,18]. The exact function of individual subunits in the PRC1 complex is not fully
58 understood, though it is suggested that they are involved in maintaining the integrity of the complex,
59 in providing or controlling enzymatic activity or in targeting to chromatin. For example, the H2AK119
60 E3 ligase activity is enhanced by the dimerization of RING1A/B with either PCGF2 or PCGF4 [19-21] or
61 can be stimulated by the PCGF1-RYBP/YAF2 interaction in the case of non-canonical PRC1.1 [16,22].

62 A shRNA approach for individual PRC1 subunits in hematopoietic stem cells revealed a lack of
63 functional redundancy, suggesting unique functions of distinct PRC1 complexes [23] and indeed PRC1
64 complex composition changes upon lineage specification [24].
65
66 To better understand the function of PRC1 complexes in human leukemias, we recently identified an
67 essential role for non-canonical PRC1.1 proteins [17]. PRC1.1 was first identified by the purification of
68 the BCOR protein, which was found to interact with RING1A/B, RYBP, PCGF1, SKP1 and KDM2B
69 [25,26]. A potential oncogenic role of PRC1.1 is underlined by the fact that KDM2B is overexpressed
70 in leukemias, breast and pancreatic cancers where it functions as an oncogene, conversely
71 knockdown of KDM2B abrogated tumorigenicity [17,27-30]. Via the ZF-CxxC domain of KDM2B,
72 PRC1.1 is targeted to non-methylated CpG islands genome-wide and contributes to PRC1.1
73 recruitment [17,31-34]. The PRC1.1 complex assembles around a core PCGF1-RING1B dimer
74 [22,35,36]. While Polycomb-mediated silencing by canonical PRC1 and PRC2 complexes is thought to
75 maintain compacted chromatin, which is inhibitory to transcription [37,38], less is known about the
76 function of PRC1.1 on gene transcription. In mouse embryonic stem cells (mESCs) and mouse
77 embryonic fibroblasts it is suggested that KDM2B functions together with PRC2 to repress lineage-
78 specific genes [32,33,39]. On the other hand, Boulard and colleagues find more DNA methylation in
79 KDM2B null mESC at CpG islands co-occupied by PRC2, suggesting that KDM2B keeps promoters in an
80 activated non-methylated state [40]. We and others have shown that PRC1.1/KDM2B can also be
81 targeted to sites independent of PRC2/H3K27me3 and notably is associated with 'permissive' or
82 active chromatin suggested by the occupancy of H3K4me3, H3K36me3, RNAPII (S5P) and H3K27ac
83 [17,41-43].
84
85 A better understanding of PRC1.1 function is required in order to understand its role in gene
86 regulation and to explore possibilities to target PRC1.1 in human diseases such as leukemia. Here, we
87 investigated KDM2B/PRC1.1 in more detail with the aim to identify alternative approaches to target

88 the non-canonical PRC1.1 complex in human leukemic cells. LC-MS/MS-based proteome studies were
89 used to investigate the complete interactome of KDM2B in human leukemic cells and we identified
90 that the deubiquitinase USP7 is an essential component of PRC1.1 and is required to maintain its
91 integrity and function. As a consequence of inhibiting USP7 deubiquitinase activity the PRC1.1
92 complex disassembles and loses binding to chromatin, with a concomitant reduction in gene
93 expression of target loci. Furthermore, our data show that USP7 is essential for leukemic cells and
94 suggests that targeting of USP7 might provide an alternative therapeutic approach for leukemia.
95
96 **RESULTS**
97 **Identification of the deubiquitinase USP7 as a subunit of PRC1.1**
98 We recently identified KDM2B as a critically important factor for the survival of human leukemic
99 stem cells [17]. Therefore, we set out to study the KDM2B interactome in detail in leukemic cells.
100 Human K562 cells were transduced with KDM2B-EGFP followed by anti-EGFP pull outs and LC-MS/MS
101 analysis to identify interacting proteins. Thus, 406 KDM2B-interacting proteins were identified
102 involved in cellular processes like DNA/chromatin binding, protein binding, RNA binding and RNA
103 polymerase activity (Fig 1A and Dataset EV1). Gene Ontology analyses revealed that this list
104 contained proteins that associated with rRNA processing, mRNA splicing, translation, mRNA
105 processing, positive regulation of gene expression and DNA damage response (Fig 1B). The most
106 abundant KDM2B interaction partners were non-canonical PRC1.1 proteins (Fig 1C), including the
107 ubiquitin-specific protease 7 (USP7). Since inhibitors are available that inhibit its deubiquitinase
108 activity, we questioned whether inhibition of USP7 could be an alternative way to target leukemic
109 stem cells, in part via inhibition of PRC1.1 and therefore we continued to study the role of USP7 in
110 further detail. To validate the interaction of USP7 with PRC1.1 proteins, besides KDM2B, we also
111 performed EGFP pull outs on nuclear extracts of stable K562 cell lines expressing PCGF1-EGFP and
112 EGFP-RING1B followed by LC-MS/MS analysis (Dataset EV2). Fig 1D shows the spectral counts
113 (MS/MS counts) corrected for expected peptides based on *in silico* protein digests. Clearly, USP7 was

114 found to interact with KDM2B, PCGF1 and RING1B and all other PRC1.1 proteins were co-purified,
115 indicating that USP7 is a subunit of PRC1.1. In addition, Western blots of independent pull outs on
116 canonical PRC1 (PCGF2, PCGF4, CBX2) and non-canonical PRC1.1 (PCGF1, RING1B) were performed
117 using antibodies against USP7 and RING1B (Fig 1E). As expected, RING1B precipitated with both PRC1
118 and PRC1.1 proteins. The interaction of USP7 with RING1B and PCGF1 was confirmed by Western
119 blot while less interaction was observed with the canonical PRC1 proteins PCGF2, PCGF4 or CBX2 (Fig
120 1E and Dataset EV3).
121
122 **USP7 inhibition results in disassembly of the PRC1.1 complex**
123 Deubiquitinating enzymes (DUBs) exert a variety of important cellular functions, including the control
124 over protein stabilization or degradation, protein localization, protein activity or by modulating
125 protein-protein interactions [44]. We therefore questioned whether inhibition of the deubiquitinase
126 USP7 might affect PRC1.1 stability and function. P22077 (1-(5-((2,4-difluorophenyl)thio)-4-
127 nitrothiophen-2-yl)ethanone) has been identified as a selective inhibitor of USP7, as well as its
128 paralog USP47, using activity-based chemical proteomics [45,46]. In general, DUB inhibitors increase
129 overall protein polyubiquitination [46]. Similarly, we observed accumulation of polyubiquitinated
130 proteins in our EGFP-RING1B and PCGF1-EGFP K562 cells treated for 24h with P22077 (Fig 2A). Next,
131 we investigated the effect of USP7 inhibition on the stability of PRC1.1. EGFP pull outs were
132 performed on nuclear extracts from K562 PCGF1-EGFP and EGFP-RING1B cells treated with DMSO or
133 P22077 followed by LC/MS-MS analysis (Fig 2B and Dataset EV4). Volcano plots were generated using
134 label-free quantification (LFQ) intensities of potential interactors of EGFP-RING1B (left) and PCGF1-
135 EGFP (right) plotted as fold change difference (control/USP7i) against significance (t-test p-value).
136 Interactions with several PRC1.1 proteins, highlighted in orange, were significantly reduced in both
137 EGFP-RING1B and PCGF1-EGFP pull outs as a consequence of USP7 inhibition (Fig 2B). The ubiquitin
138 protein, UBB, was enriched in both PCGF1-EGFP and EGFP-RING1B pull outs upon P22077 treatment,
139 suggesting that these proteins or other Polycomb interaction proteins might be more ubiquitinated

140 upon USP7 inhibition. In addition we analysed the intensity-based absolute quantification (iBAQ)
141 values, as a measure for protein abundance, relative to either RING1B or PCGF1 and normalized to
142 control pull outs (Fig 2C). Similarly, these data demonstrated a clear reduced interaction of PRC1.1
143 proteins with RING1B and PCGF1 after P22077 treatment. Independent EGFP pull outs performed on
144 PCGF1-EGFP and EGFP-RING1B cell lines further confirmed that USP7 inhibition indeed resulted in
145 reduced interaction of PCGF1-EGFP with endogenous RING1B and EGFP-RING1B with endogenous
146 PCGF1 (Fig 2D). Importantly, input samples did not reveal loss of protein stability and also the
147 expression of EGFP-RING1B and PCGF1-EGFP was not affected as quantified by FACS analysis (Fig 2E).
148 Taken together these data indicate that USP7 is essential for PRC1.1 complex integrity.
149
150 **PRC1.1 chromatin binding relies on functional USP7 deubiquitinase activity**
151 To determine the functional consequences of disassembly of the PRC1.1 complex upon USP7
152 inhibition, we performed several ChIPs to investigate whether PRC1.1 would still be recruited to
153 target loci. Previously, we identified PRC1 and PRC1.1 target loci by ChIP-seq for PCGF1/2/4, CBX2,
154 RING1A/1B, KDM2B, H2AK119ub and H3K27me3 in the leukemic cell line K562 [17]. Here, ChIP-
155 qPCRs were performed for KDM2B, PCGF1 and RING1B, the core PRC1.1 subunits, on several loci in
156 the absence or presence of P22077 (30 µM). Inhibition of USP7 resulted in a complete loss of KDM2B
157 binding, with concomitant strong reductions in PCGF1 and RING1B chromatin binding (Fig 3A).
158 Importantly, USP7 inhibition did not result in reduced protein levels of KDM2B, PCGF1 or RING1B (Fig
159 2D and E and Fig EV1). Since RING1B mediates H2AK119 ubiquitination we then analysed the levels of
160 this histone modification upon USP7 inhibition. Similarly, H2AK119ub was lost from PRC1.1 target loci
161 (Fig 3B). These data suggest that USP7 inhibition severely impacts on PRC1.1 chromatin binding and
162 likely as a consequence on H2AK119ub levels. Since non-canonical PRC1.1 can be recruited to active
163 loci in leukemic cells, we also investigated the levels of H3K4me3, but no changes were observed on
164 this histone mark upon USP7 inhibition, further highlighting that not all posttranslational histone
165 modifications are affected as a consequence of treatment (Fig 3C). To test whether the loss of

166 H2AK119ub would indeed be the result of impaired *de novo* ubiquitination by either one of the two
167 E3 ligases RING1A/1B, cells were cross-linked at 4h, 8h and 16h followed by a ChIP for H2AK119ub,
168 KDM2B and RING1B (Fig 3D). The time-dependent loss of H2AK119ub coincided with a loss of KDM2B
169 and RING1B binding at the same target loci, suggesting that loss of *de novo* ubiquitination underlies
170 these observations. Again, H3K4me3 levels remained unaffected, while H3K27ac levels were reduced
171 upon USP7 inhibition indicative for reduced transcriptional activity at these loci (Fig 3E). We then
172 performed genetic knockdown studies of USP7 as an alternative approach to study its function (Fig
173 EV2A). ChIP-qPCR experiments showed reduced KDM2B chromatin binding to PRC1.1 loci by two
174 independent miR-E USP7 shRNAs, although this reduction was less compared to cells treated with
175 the USP7 inhibitor (Fig EV2B). Presumably our shRNA approach did not result in a complete loss of
176 USP7 expression, resulting in some USP7 catalytic activity remaining intact. To address this further
177 we also included a new recently developed compound in our studies, FT671, which was shown to
178 inhibit USP7 with high affinity and specificity [47]. We performed KDM2B and H2AK119ub ChIPs in
179 the absence or presence of FT671 and also these data clearly demonstrated a loss of KDM2B binding
180 and reduced H2AK119ub levels to PRC1.1 loci upon inhibiting USP7 function (Fig 3F).
181
182 **USP7 inhibition leads to downregulation of several PRC1.1 active target genes**
183 Given that USP7 inhibition severely impaired PRC1.1 occupancy to several target loci we investigated
184 whether this would also affect the expression of PRC1.1 target genes in leukemic cells. RNA-seq was
185 performed to compare gene expression in DMSO or USP7 inhibitor treated K562 cells (P22077, 30
186 µM) for 4h, 8h, 16h and 24h. Since PRC1.1 can be associated with active genes in leukemic cells we
187 focused on the genes that were downregulated upon USP7 inhibition. In total 297 genes were
188 downregulated more than 2 fold after 24h of USP7 inhibition (Dataset EV5). Since USP7 has also
189 PRC1.1 independent functions, for instance by controlling MDM2/p53 [48], we then analysed
190 whether downregulated genes overlapped with previously identified PRC1.1 peaks by ChIP-seq (Fig
191 4A, Dataset EV5)[17]. Twenty-four percent of these genes overlapped with PRC1.1 targets. Gene

192 Ontology (GO) analysis revealed that this set was enriched for GO terms like transcription, regulation
193 of gene expression and chromatin modification, while PRC1.1 independent downregulated genes
194 were enriched for GO terms like mRNA splicing, protein folding and protein polyubiquitination (Fig
195 4A). ChIP-seq profiles of TOP2B, SIN3A, CHD1 and MYC are shown in Fig 4B as representative
196 examples for PRC1.1 target genes. The tracks show clear binding of PCGF1, RING1A/1B and KDM2B
197 and little occupancy of canonical PRC1 proteins (PCGF2, PCGF4, CBX2). These loci were also enriched
198 for H2AK119ub and active chromatin marks H3K4me3, H3K36me3, RNAPII and H3K27ac but devoid
199 of the repressive mark H3K27me3. Loss of PRC1.1 binding was confirmed by ChIP-qPCRs for KDM2B,
200 PCGF1 and RING1B on these 4 loci (Fig 4C). Again, a concomitant loss of H2AK119ub and H3K27ac
201 marks was seen, without any alterations in H3K4me3 (Fig 4C). Subsequently, the observed
202 downregulation based on RNA-seq data was validated by independent quantitative RT-PCRs (Fig 4D).
203 Loss of PRC1.1 binding correlated with loss of gene expression. Taken together, these data suggest
204 that the presence of PRC1.1 is required to maintain the transcriptional activity of several target
205 genes.
206
207 **Both quiescent and cycling primary AML cell populations are sensitive towards USP7 inhibition**
208 To study the functional consequences of USP7 inhibition, we tested P22077 on the AML cell lines
209 MOLM-13, NB4, K562 and HL60. USP7 inhibition severely impaired cell growth in all tested AML cell
210 lines (Fig 5A) associated with increased apoptosis. Also the specific USP7 inhibitor (FT671)
211 demonstrated reduced proliferation of MOLM-13, OCI-AML3, K562 and HL60 cells (Fig 5B). Cell lines
212 that do not express functional p53 (HL60 and K562) also showed sensitivity, indicating that at least in
213 those cell lines the effect of P22077 and FT671 was independent of p53 (Dataset EV6). Next, we
214 assessed whether USP7 inhibition, using P22077, also affected the survival of primary AML cells. The
215 long-term proliferation of primary AML $CD34^+$ cells (n=3) on MS5 co-culture was clearly reduced in
216 the presence of P22077 (Fig 5C). Patient characteristics are shown in Dataset EV6. With current
217 therapies for leukemia patients the majority of the blast population is readily eradicated, while the

218 rare quiescent population of leukemic stem cells is more difficult to target. To examine the effects of
219 USP7 inhibition (P22077) on both cycling as well as quiescent (G_0) cells, we performed
220 Hoechst/PyroninY stainings. AML 2 was characterized by a large $CD34^+/CD38^+$ population that is high
221 in cycling activity, while the $CD34^+/CD38^-$ population is predominantly in G_0 (Fig 5D). In both
222 populations, the G_0 fraction was equally or even more efficiently targeted by P22077 compared to
223 the cycling fraction, indicating that cycling cells are not necessarily more sensitive than quiescent
224 cells. AML3 was low in $CD34^+$ and therefore we gated on the whole blast population which also
225 showed that both quiescent and cycling cells were sensitive for P22077 (Fig 5E).
226
227 **Evaluation of USP7 inhibition in a xenograft leukemia mouse model**
228 Next, we evaluated the effect of USP7 inhibition in our human CB MLL-AF9 xenograft mouse model
229 (Fig 6A) [49,50]. Importantly, these lymphoid MLL-AF9 cells grown on a co-culture of MS5 *in vitro*
230 were sensitive towards USP7 inhibition (Fig EV3). Here 5 x 10^4 MLL-AF9 leukemic cells, from a
231 primary leukemic mouse, were intravenously (IV) injected into secondary recipients (n=11). Three
232 weeks after injection 10/11 mice showed engraftment of MLL-AF9 $EGFP^+/CD45^+/CD19^+$ cells in
233 peripheral blood (Fig 6B). Subsequently, mice were divided into two groups that were treated either
234 with DMSO as control (n=5) or 20 mg/kg P22077 (n=6) via intraperitoneal (IP) injections. Peripheral
235 blood chimerism levels were monitored by regular blood sample analysis and mice were sacrificed
236 when chimerism levels in the blood exceeded 40%. Mice were treated daily starting four weeks post-
237 transplant (indicated with the arrow, Fig 6C). Two-and-a-half weeks after starting treatment,
238 chimerism levels were significantly lower in P22077-treated mice compared to DMSO (Fig 6B and C).
239 The chimerism levels for DMSO treated mice rapidly increased to 44% (average) within 6 weeks after
240 injection, whereas the chimerism levels of P22077 treated mice were around 25% on average.
241 Notably, 3/6 mice gave a better response to USP7 inhibition with lower chimerism levels of 18.3, 16.8
242 and 12% respectively at day 46 (Fig 6B). Upon treatment we followed the mice for some additional
243 weeks and within 60 days all control mice exceeded 40% chimerism in the blood, indicative for a full

244 blown leukemia and were sacrificed (Fig 6C and D). Bone marrow, spleen and liver analyses showed
245 high levels (>90%) of chimerism. USP7 inhibition delayed leukemia development and in particular in
246 two mice a clear response to USP7 inhibition was observed and chimerism levels remained relatively
247 stable between day 56-67 post-transplant, although ultimately mice did develop MLL-AF9 induced
248 leukemia after day 77 (Fig 6D).
249 Since the efficacy of USP7 inhibition *in vitro* in AML cell lines and patient samples was rather high, in
250 contrast to what we observed *in vivo* in our xenograft mouse model, we hypothesized that the bone
251 marrow niche could potentially play a protective role in the survival of leukemic cells and dampen
252 the response to therapeutic agents [51-53]. Therefore we evaluated the efficacy of USP7 inhibition in
253 a direct comparison of CB MLL-AF9 cells grown in liquid culture or in a co-culture setting on murine
254 MS5 bone marrow stromal cells. In both settings P22077 impaired cell growth, but the efficacy was
255 much higher in liquid culture conditions (Fig 6E). Loss of KDM2B binding to PRC1.1 target loci was
256 confirmed by ChIP-qPCRs, both under liquid culture and MS5 co-culture conditions, although we did
257 note that the efficacy was somewhat higher under liquid culture conditions (Fig 6F).
258
259
260

261 **DISCUSSION**

262 In this study, we reveal that the deubiquitinase USP7 is an essential component of non-canonical
263 PRC1.1 in leukemia and is required for its stability and function. Inhibiting USP7 deubiquitinase
264 activity resulted in disassembly of the PRC1.1 complex. Consequently, recruitment of the PRC1.1
265 complex to target loci was heavily lost coinciding with the loss of its H2AK119ub catalytic activity.
266 This causes repression of a subset of transcriptionally active PRC1.1 target genes and corresponds
267 with a reduction in H3K27ac, highlighting an essential function for PRC1.1 in maintaining gene
268 transcription. Furthermore, USP7 inhibition strongly impaired leukemic cell growth *in vitro* and
269 delayed MLL-AF9 induced leukemia *in vivo*, although in a niche-dependent manner.

270 The non-canonical PRC1.1 complex consists of several Polycomb proteins and although we begin to
271 learn more about the function of some of the individual proteins within the complex, the role that
272 others fulfill remains far from completely understood. PRC1.1 is recruited to non-methylated CpG
273 islands via KDM2B and a single point mutation in the ZF-CxxC domain (K643A) of KDM2B has been
274 shown to prevent this interaction [31,32,34]. The H2AK119 E3 ubiquitin ligase activity of both
275 canonical PRC1.2/1.4 and non-canonical PRC1.1 is mediated by RING1A/1B proteins and is supported
276 by the dimerization with one of the PCGFs (PCGF1-6) [54-56]. For example, non-canonical
277 PCGF1/3/5/6-RING1 heterodimers show much higher E3 ligase activity than canonical PCGF2/4-
278 RING1 heterodimers [54]. This difference possibly lies in a structural difference in PCGF helix α3
279 residues between canonical and non-canonical PCGFs which may limit ubiquitin transfer by the
280 RING1 dimer. Furthermore, the interaction of RYBP/YAF2 with the PCGF1-RING1B core dimer
281 increased the relative H2AK119 E3 ligase activity of PRC1.1 in an *in vitro* assay [22]. KDM2B and BCOR
282 contributed little or nothing to this activity.

283 A role for the deubiquitinase USP7 within PRC1.1 was suggested since USP7 stably interacts with
284 PRC1.1 proteins, KDM2B, PCGF1 and RING1B (Fig 1). Sánchez and colleagues first identified the
285 ubiquitin protease USP7 as an interactor of RING1B [26]. Then, USP7 was also identified in
286 proteomics analysis of PCGF1, RYBP, YAF2 and RING1A/B pullouts [16,17]. Previously, USP7 has been

287 shown to be associated with the canonical PRC1 protein BMI1 (PCGF4) and potentially also with
288 MEL18 (PCGF2), although Lecona and colleagues suggested that USP7 interacts directly with SCML2
289 and thereby bridges the interaction with PRC1.4 [57,58]. Similar to Gao and colleagues [16] however,
290 in our canonical PCGF2, PCGF4 and CBX2 proteome analyses we found little or no interaction with
291 USP7 [17]. We did notice that several canonical RING1B-Polycomb interactions were also reduced
292 upon USP7 inhibition, including CBX2/4/8, SCML2 and SCMH1, though the interaction with PCGF2
293 and PCGF4 was not affected. This might also suggest that USP7 impacts on PRC1 protein stability,
294 although further studies are required to clarify these issues. In line with that notion, a recent paper
295 demonstrated that another deubiquitinase, USP26, controls the stability of CBX4 and CBX6 and
296 thereby affects the complex composition of PRC1 during ESC reprogramming [59]. Maertens and
297 colleagues demonstrated that also USP11 interacts with PRC1 proteins and affects the stability of
298 BMI1 [58]. Thus, DUBs reveal an interesting role on Polycomb stability and complex composition.
299 Based on our observations, the complex composition of PRC1.1 is affected upon USP7 inhibition. This
300 suggest that controlling ubiquitin levels of Polycomb proteins is important for the integrity of the
301 protein-protein interactions within PRC1.1 and its chromatin binding. Upon USP7 inhibition an overall
302 increase in protein ubiquitination was observed (Fig 2). Importantly, USP7 inhibition did not lead to
303 degradation of PCGF1 or RING1B, allowing us to conclude that USP7 controls protein-protein
304 interactions rather than proteasomal degradation. In line with that notion, overexpression of USP7
305 has been shown to deubiquitinate RING1B thereby stabilizing RING1B and preventing it from
306 proteasomal degradation [60]. Furthermore, RING1B self-ubiquitination is required for its ligase
307 activity on histone H2A [61]. This is supported by the observation that H2AK119ub is lost upon USP7
308 inhibition, most likely as a consequence of loss of *de novo* ubiquitination mediated via RING1B.
309 Similarly, knockout of USP7 reduced H2AK119ub levels coinciding with reduced levels of RING1B [57].
310 Other studies also show that USP7 is not likely a DUB for H2AK119 [58,62,63]. Thus, regulating
311 ubiquitin levels within the PRC1.1 complex itself is critically important and mediated via USP7
312 deubiquitinase activity.

313 With the efficient loss of PRC1.1 binding and consequent loss of H2AK119ub from target loci upon
314 USP7 inhibition we were able to study PRC1.1 function in relation to gene regulation in more detail.
315 Previously we identified genes that are targeted by PRC1.1 independent of H3K27me3 and have a
316 transcriptionally active profile suggested by H3K4me3, RNAPII and H3K27ac occupancy close to the
317 transcription start site. Loss of PRC1.1 binding resulted in reduced gene expression coinciding with
318 reduced levels of H3K27ac in the majority of analysed cases. The mechanisms underlying differences
319 in gene expression when PRC1.1 binding is lost are currently unclear. We hypothesize that PRC1.1
320 creates a transcriptionally permissive and open chromatin state which enables transcription factors
321 to bind and initiate gene expression. Addressing a possible cross-talk between PRC1.1 proteins,
322 CBP/p300-linked H3K27ac, recruitment of transcription factors and accessibility of chromatin is
323 definitely a focus for future work. Since H3K4me3 levels remained unaffected following USP7
324 inhibition, this suggest that the H3K4 methyltransferase complex that is likely targeted to CpGs via
325 CFP1 protein is not targeted in a PRC1.1-dependent manner [64].
326 In ESCs PRC1.1 targets are usually described together with canonical PRC1/PRC2 signaling, known as
327 bivalent loci and shown to repress target genes [31-33]. For example, knockdown of KDM2B leads to
328 the up-regulation of a subset of poised target genes, coinciding with some reduction in RING1B
329 binding and H2AK119ub [31]. While we find no clear interaction of USP7 with canonical PRC1 in
330 leukemic cells, it was shown that USP7 inhibition does impact functionally on canonical PRC1 [57].
331 Inhibiting the catalytic core by removal of RING1A/B in ESCs does not lead to loss of KDM2B binding
332 [31]. However, in leukemic cells we find that USP7 inhibition not only leads to reduced H2AK119ub
333 but also induces loss of PRC1.1/KDM2B binding as a result of complex disassembly, suggesting that
334 KDM2B-PCGF1-BCOR/L1/SKP1 interactions might be needed for targeting. This is in agreement with
335 data that suggest that dimerization of PCGF1 and BCOR(L1) is required for binding to KDM2B and
336 recruiting PRC1.1 to the chromatin [35].
337 PRC1.1 is essential for human leukemic cells [17]. By inhibiting individual Polycomb proteins using an
338 shRNA approach we observed impaired cell growth of leukemic cells upon knockdown of PCGF1,

339 RING1B, KDM2B or BCOR. *In vivo* experiments in humanized niche xenograft mice using primary AML
340 patient samples [65] or lentiviral leukemia models [50] demonstrated that leukemogenesis was
341 delayed or even abrogated upon knockdown of PRC1.1 proteins. While these genetic studies clearly
342 highlight the importance of PRC1.1 for the survival of leukemic cells, small molecule inhibitors would
343 be easier to implement in a therapeutic clinical setting. Various USP7 inhibitors have been
344 developed, and most recently selective USP7 inhibitors which destabilize USP7 substrates including
345 MDM2 and thereby increase p53-mediated apoptosis of cancer cells were generated [47,66]. We
346 observed that leukemic cells were very sensitive to USP7 inhibition, both in model systems as well as
347 in primary patient samples. Importantly, also the quiescent leukemic cells, that are usually more
348 difficult to target, showed sensitivity to P22077. It is evident that USP7 can function in several
349 pathways, often through regulating protein stability of tumor suppressors or epigenetic regulators
350 [67-69] and it is particularly the p53 pathway that is strongly controlled by USP7 [70-73]. While we
351 cannot exclude the possibility that some of these pathways were also affected in some of our
352 studies, we have analysed the p53 status in our models and primary AML patient samples and see
353 sensitivity even in the absence of a normal p53 response. Furthermore, while USP7 knockout mice
354 are embryonically lethal, deletion of p53 was not able to rescue this phenotype, further highlighting
355 that p53-independent pathways downstream of USP7 exist as well [74]. Although P22077 has shown
356 antitumor effects *in vivo* in neuroblastoma models [70,75], the responses that we observed *in vivo* in
357 our CB MLL-AF9 leukemia model were more modest, despite very strong effects seen upon USP7
358 inhibition *in vitro*. We wondered whether the presence of a protective bone marrow
359 microenvironment might play a role in regulating P22077 sensitivity and therefore performed
360 experiments in the absence or presence of bone marrow stroma. We indeed demonstrate that MLL-
361 AF9 cells grown on MS5 stromal cells were less sensitive towards USP7 inhibition compared to cells
362 grown in liquid culture conditions. These observations are in line with other data clearly supporting
363 the notion that the niche plays a protective role and can dampen the response to therapeutic agents
364 [51-53].

365 In conclusion, our data reveal an important role for USP7 deubiquitinase activity in the integrity of
366 the PRC1.1 complex. We provide insight into the recruitment of PRC1.1 to target loci and function in
367 gene regulation and show that PRC1.1 is a potential interesting therapeutic target in leukemia.
368

369 **MATERIALS AND METHODS**

370 **GFP-mediated pull outs**

371 Pull outs were performed on nuclear extracts from K562 cells stably expressing KDM2B-EGFP, PCGF1-
372 EGFP and EGFP-RING1B. At least $80x10^6$ cells were collected for each pull out, washed with PBS and
373 lysed in 3 ml buffer A including freshly added protease inhibitors (10 mM HEPES/KOH pH 7.9, 1.5 mM
374 MgCl2, 10 mM KCl, 1 mM DTT, 1x Chymostatin Leupeptin Antipain Pepstatin (CLAP) protease-
375 inhibitor cocktail (all 1 µg/ml) and 0.1 mM PMSF (all from Sigma-Aldrich). After 10 minutes
376 incubation on ice, 10% IGEPAL CA-630 (endconc. 0.5%, Sigma-Aldrich) was added, followed by 10
377 seconds vortexing and 1 minute 14000 rpm spin to recover the nuclei. Nuclei were resuspended in
378 0.7 ml high salt buffer (20 mM HEPES/KOH pH 7.9, 1.5 mM MgCl2, 420 mM NaCl, 0.2 mM EDTA, 25%
379 Glycerol, 1 mM DTT, 1x CLAP and 0.1 mM PMSF) and incubated on ice for 20 minutes with 10
380 seconds vortexing intervals every 5 minutes. Extracted nuclei were collected after 15 minutes at
381 14000 rpm at 4°C and 2 volumes of Dilution buffer (25 mM Tris/Cl pH 7.5, 0.45% IGEPAL CA-630, 1 x
382 CLAP, 0.1 mM PMSF) and 3 volumes Wash buffer (TBS, 0.3% IGEPAL CA-630, 1 x CLAP, 0.1 mM PMSF)
383 were added. Pre-clearing of cell lysate was done by adding 50 µl pre-equilibrated binding control
384 magnetic agarose beads (Chromotek) and incubated for 30 min at 4°C on a rotating platform. Then
385 pre-cleared lysate was incubated with 70 µl pre-equilibrated GFP-Trap magnetic agarose beads
386 (Chromotek) overnight at 4°C on a rotating platform. Beads were separated using a magnetic rack
387 and six times washed in Wash buffer. Bound (B) fractions were eluted from the beads by boiling for
388 10 min in 2x Leammli sample buffer.
389
390

391 **In gel trypsin digestion**

392 Bound fractions of KDM2B-EGFP, PCGF1-EGFP (control/USP7i) and GFP-RING1B (control/USP7i) were
393 loaded on a 4-12% pre-cast NuPAGE gel (Invitrogen) and were run briefly. Gels were stained with
394 Coomassie dye R-250 (Thermo Scientific) and subsequently destained with ultrapure water
395 overnight. Gel lanes were cut into one slice, further cut into small pieces and completely destained
396 using 70% 50 mM NH_4HCO_3 and 30% acetonitrile (ACN). Reduction and alkylation of cysteines was
397 performed by adding 10 mM DTT dissolved in 50 mM NH_4HCO_3 and incubated at 55°C for 30 min.
398 Next, 55 mM iodoacetamide in 50 mM NH_4HCO_3 was added and incubated for 30 min, in dark, at
399 room temperature. Remaining fluid was removed and 50 mM NH_4HCO_3 was added with 10 min.
400 shaking. Then 100% ACN was added incubated for 30 min. while shaking. Fluid was removed and gel
401 pieces were dried for 15 min. at 55°C. Proteins were digested with adding 10 ng/µl sequencing-grade
402 modified trypsin (Promega) in 50 mM NH_4HCO_3 to the gel pieces and incubated overnight at 37°C.
403 Next day, peptides were extracted using 5% formic acid followed by second elution with 5% formic
404 acid in 75% acetonitrile. Samples were dried in a SpeedVac centrifuge and dissolved in 5% formic
405 acid.

406

407 **LC-MS/MS analysis**

408 Online chromatography of the extracted tryptic peptides was performed with the Ultimate 3000
409 nano-HPLC system (Thermo Fisher Scientific) coupled online to a Q-Exactive-Plus mass spectrometer
410 with a NanoFlex source (Thermo Fisher Scientific) equipped with a stainless steel emitter. Tryptic
411 digests were loaded onto a 5 mm × 300 µm i.d. trapping micro column packed with PepMAP100 5
412 µm particles (Dionex) in 0.1% FA at the flow rate of 20 µL/min. After loading and washing for 3
413 minutes, peptides were forward-flush eluted onto a 50 cm × 75 µm i.d. nanocolumn, packed with
414 Acclaim C18 PepMAP100 2 µm particles (Dionex). The following mobile phase gradient was delivered
415 at the flow rate of 300 nL/min: 2–50% of solvent B in 90 min; 50–80% B in 1 min; 80% B during 9 min,
416 and back to 2 % B in 1 min and held at 3% A for 19 minutes. Solvent A was 100:0 H2O/acetonitrile

417 (v/v) with 0.1% formic acid and solvent B was 0:100 H2O/acetonitrile (v/v) with 0.1% formic acid. MS
418 data were acquired using a data-dependent top-10 method dynamically choosing the most abundant
419 not-yet-sequenced precursor ions from the survey scans (300–1650 Th) with a dynamic exclusion of
420 20 seconds . Sequencing was performed via higher energy collisional dissociation fragmentation with
421 a target value of 2e5 ions determined with predictive automatic gain control. Isolation of precursors
422 was performed with a window of 1.6. Survey scans were acquired at a resolution of 70,000 at m/z
423 200. Resolution for HCD spectra was set to 17,500 at m/z 200 with a maximum ion injection time of
424 110 ms. The normalized collision energy was set at 28. Furthermore, the S-lens RF level was set at 60
425 and the capillary temperature was set at 250degr. C. Precursor ions with single, unassigned, or six
426 and higher charge states were excluded from fragmentation selection.
427
428 **Data analysis**
429 Raw mass spectrometry data were analysed using MaxQuant version 1.5.2.8 [76], using default
430 settings and LFQ/ iBAQ enabled, searched against the Human Uniprot/Swissprot database
431 (downloaded June 26, 2016, 20197 entries). Further data processing was performed using Perseus
432 software, version 1.5.6.0 [77]. Network visualization of KDM2B interactome was performed using
433 Cytoscape software, version 3.5.1. For Gene Ontology (GO) analysis we used DAVID Bioinformatics
434 Resources (http://david.abcc.ncifcrf.gov/home.jsp). ChIP-seq tracks were visualized and analysed
435 using UCSC genome browser (http://genome.ucsc.edu). Accession number for the Polycomb ChIP-
436 seq data previously reported and used for analysis in this paper is GEO: GSE54580 [17]. Previously
437 published ChIP-seq used for analysis include H3K4me3, H3K36me3, H3K27ac and RNAPII/Pol2(b)
438 from ENCODE/Broad Institute (GSE29611).
439
440 **Patient samples**
441 AML blasts from peripheral blood or bone marrow from untreated patients were studied after
442 informed consent and the protocol was approved by the Medical Ethical Committee, in accordance

443 with the Declaration of Helsinki. Mononuclear cells were isolated by density gradient centrifugation
444 and CD34+ cells were selected automatically by using autoMACS (Miltenyi Biotec).
445
446 **Cell culture**
447 The AML cell lines K562, MOLM13, NB4, OCI-AML3 and HL-60 were cultured in RPMI 1640
448 (BioWhittaker, Lonza, Verviers, Belgium) supplemented with 10% fetal bovine serum (FCS, HyClone
449 Laboratories, Logan, Utah, US) and 1% penicillin/streptomycin (p/s, PAA Laboratories). MS5 murine
450 stromal cells were cultured in alpha-MEM with 200 mM glutamine (BioWhittaker) supplemented
451 with 10% FCS and 1% p/s. Primary AMLs were cultured in Gartner's medium consisting of alpha-MEM
452 (BioWhittaker) supplemented with 12.5% heat-inactivated FCS and 12.5% heat-inactivated Horse
453 serum (Sigma-Aldrich, Saint Louis, MO, USA), 1 µM hydrocortisone (Sigma-Aldrich), 57.2 µM β-
454 mercaptoethanol (Sigma) and 1% p/s in the presence of 20 ng/ml granulocyte colony-stimulating
455 factor (G-CSF), thrombopoietin (TPO) and IL-3. All AMLs were grown on a MS5 stromal layer. CB MLL-
456 AF9 liquid and MS5 co-cultures under myeloid permissive conditions were grown in Gartner's
457 medium supplemented with 20 ng/ml Flt-3L, stem cell factor (SCF) and IL-3 [49,50]. For lymphoid CB-
458 MLL-AF9 cells were grown on MS5 co-culture in Gartner's medium without Horse serum and
459 hydrocortisone and no IL-3 was added. Instead ascorbic acid (50 µg/ml, Sigma) and IL-7 (10 ng/ml)
460 were added. All cultures were kept at 37°C and 5% CO_2. For USP7 inhibition experiments, P22077 (1-
461 (5-((2,4-difluorophenyl)thio)-4-nitrothiophen-2-yl)ethanone) was purchased from Merck Millipore
462 (662142) (Billerica, MA, USA) and stock solution dissolved in DMSO then added 1:1000 to the culture.
463 FT671 was generously provided by FORMA Therapeutics (Watertown, MA, USA)[47].
464
465 **Generation of lentiviral vectors and transductions**
466 Lentiviral pRRL SFFV PCGF1-EGFP and EGFP-RING1B vectors were generated as described
467 previously[17]. pRRL SFFV KDM2B EGFP was generated as follows. KDM2B was PCR amplified from
468 cDNA in two parts (from the ATG to the RsrII site [fragment 1] and from the RsrII site to end of

469 KDM2B [excluding the stop codon, fragment 2]). Both fragments were independently subcloned into
470 pJet1.2 resulting in the pJet1.2 KDM2B[1] and pJet1.2 KDM2B[2] plasmids and that were
471 subsequenty verified by sequencing. Next, KDM2B fragment 2 was isolated from pJet1.2 KDM2B[2]
472 using RsrII and XbaI digestion and ligated into pJet1.2 KDM2B[1] that was also digested with RsrII and
473 XbaI, resulting in a pJet1.2 plasmid with the full length KDM2B ORF but excluding the stop codon.
474 Finally, the KDM2B ORF was subcloned into the pRRL SFFV GFP vector using AgeI digestion, resulting
475 in the pRRL SFFV KDM2B-GFP construct. A lentiviral pRRL SFFV-His-Ubiquitin-mBlueberry2 vector was
476 generated by PCR amplification of His-Ubiquitin from pCl His-Ubi (Addgene) plasmid using primers
477 including BamHI sites. The PCR product was first ligated into pJet1.2 using Blunt-End cloning
478 protocol. Subsequently His-Ubiquitin was isolated from pJet1.2 using BamHI digestion and ligated
479 into pRRL SFFV-IRES-mBlueberry2 vector also using BamHI digestion and verified by sequencing.
480
481 The constitutive lentiviral pRRL.SFFV.EGFP.miR-E vector was generated by subcloning the EGFP.miR-E
482 from the pRRL LT3GECIR vector (generously provided by the Zuber lab) into the
483 pRRL.SFFV.IRES.EGFP[78]. Therefore the LT3GECIR vector was cut with MluI and self-ligated. The
484 pRRL.SFFV.IRES.EGFP vector was cut with XhoI and EcoRI (Klenow) followed by self-ligation. The
485 EGFP.miR-E was isolated from the LT3GECIR vector with BamHI and SacII digestion and cloned into
486 the pRRL.SFFV.IRES.EGFP cut with BamHI and SacII, resulting into the pRRL.SFFV.EGFP.miR-E vector.
487 Subsequently miR-E shRNAs for USP7 and a SCR control were designed or selected from Table S3
488 (Fellmann et al, 2013). USP7 #A: TGCTGTTGACAGTGAGCGACAGGATTTATTCAAGATACTATAGTGAAGCC
489 ACAGATGTATAGTATCTTGAATAAATCCTGCTGCCTACTGCCTCGGA; USP7#B:TGCTGTTGACAGTGAGCGCC
490 AAGAACATTGTTAAATTCAATAGTGAAGCCACAGATGTATTGAATTTAACAATGTTCTTGATGCCTACTGCCTC
491 GGA; SCR: TGCTGTTGACAGTGAGCGCAGGAATTATAATGCTTATCTATAGTGAAGCCACAGATGTATAGATA
492 AGCATTATAATTCCTATGCCTACTGCCTCGGA . 97-mer oligonucleotides were purchased from
493 Invitrogen and PCR amplified using the primers miRE-Xho-fw (5'
494 TGAACTCGAGAAGGTATATTGCTGTTGACAGTGAGCG-3') and miRE-EcoOligo-rev (5'-

495 TCTCGAATTCTAGCCCCTTGAAGTCCGAGGCAGTAGGC-3′) according to Phusion High-Fidelity kit
496 (Thermo Scientific). The PCR product (139 bp) was first ligated into pJet1.2 using Blunt-End cloning
497 protocol and verified by sequencing. Then the miR-E shRNA was isolated using XhoI and EcoRI
498 digestion and ligated into the pRRL.SFFV.EGFP.miRE vector also using XhoI and EcoRI digestion.
499 Generation of lentiviral viruses and transductions were performed as described previously [79].
500
501 **Flow cytometry analysis**
502 Flow cytometry analyses were performed on the BD LSR II (Becton Dickinson (BD) Biosciences) and
503 data were analysed using FlowJo (Tree Star Inc, Ashland, OR, USA). Cells were sorted on a MoFlo XDP
504 or MoFLo Astrios (Beckman Coulter). For Hoechst/PyroninY staining, cells were resuspended in
505 HPGM (Lonza, Leusden, The Netherlands) and stained with 5 ug/ml Hoechst 33342 (Invitrogen) at
506 37°C for 30-45 min. Then 1 ug/ml PyroninY (Sigma) was added and incubated for 30-45 min at 37C.
507 Upon FcR blocking (MACS miltenyi Biotec), cells were stained with CD34-APC (581, BD Biosciences)
508 and CD38-AlexaFluor 700 (HIT2, Biolegend) at 4°C for 30 min. Cells were washed in medium
509 containing Hoechst/PyroninY and analysed on the BD LSR II. *In vivo* engraftment levels were analysed
510 in peripheral blood (PB), bone marrow, liver and spleen. Prior to staining, cells were blocked with
511 anti-human FcR block (MACS miltenyi Biotec) and anti-mouse CD16/CD32 block (BD Biosciences) and
512 stained with CD45-BV421 (HI30), CD19-BV785 (HIB19) and CD33-APC (WM53) all from Biolegend at
513 4°C for 30 min.
514
515 **Western blotting**
516 For detecting His-tagged ubiquitinated proteins cells were lysed in 1 ml denaturing lysis buffer (6M
517 Guanidium-HCl, 100 mM Na_2HPO_4 x $2H_2O$, 10 mM Tris-HCl pH 8.0, 5 mM Imidazole, 10 mM β-
518 mercaptoethanol) and sonicated on ice. Lysates were pre-cleared by centrifugation at 14000 rpm at
519 4°C and five volumes denaturing lysis buffer was added. His-tagged ubiquitinated proteins were
520 purified by adding 75 µl pre-equilibrated Ni-NTA magnetic agarose beads (Jena Bioscience) and

521 incubated for 4h on a rotating wheel. Beads were separated using a magnetic rack and washed 1x in
522 denaturing lysis buffer without Imidazole, 1x in wash buffer pH 8.0 (8M Urea, 100 mM Na_2HPO_4 x
523 $2H_2O$, 10 mM Tris-HCl pH 8.0 and 10 mM β-mercaptoethanol), 1x in wash buffer pH 6.3 (8M Urea,
524 100 mM Na_2HPO_4 x $2H_2O$, 10 mM Tris-HCl pH 6.3, 10 mM β-mercaptoethanol) plus 0.2% Triton X-100,
525 and 1x in wash buffer pH 6.3 plus 0.1% Triton X-100. His-tagged ubiquitinated proteins were eluted
526 from the beads by adding 75 µl elution buffer (200 mM Imidazole, 150 mM Tris-HCl pH 6.7, 30%
527 glycerol, 5% SDS and 720 mM β-mercaptoethanol) and incubated for 20 min. on a rotating wheel.
528 Elution samples were diluted 2x in Laemmli sample buffer containing 10% β-mercaptoethanol and
529 immediately boiled for 5 min. prior to Western blot analysis.
530 GFP mediated pull out cell lysates, input, non-bound and bound fractions were boiled for 5-10 min. in
531 Laemmli sample buffer prior to SDS-polyacrylamide gel electrophoresis. Proteins were transferred to
532 fluorescence polyvinylidene difluoride (PVDF FL, Millipore) membrane by semidry blotting.
533 Membranes were blocked in Odyssey blocking buffer (Westburg). The following primary antibodies
534 were used: anti-USP7 (A300-033A, Bethyl Laboratories), anti-RING1B (ab 181140, Abcam), anti-GFP
535 (sc-9996, Santa Cruz), anti-Ubiquitin (FK2, Enzo Life Sciences), anti-PCGF1 (ab183499, Abcam).
536 Fluorescent secondary antibodies either goat anti-mouse IRDye 800 or goat anti-rabbit IgG (H+L)
537 Alexa Fluor 680 (Invitrogen) were used for detection. Membranes were scanned using the Odyssey
538 CLx Imaging System (Li-Cor Biosciences).
539
540 **Chromatin immunoprecipitation**
541 ChIP was essentially performed as described previously (Frank, 2001), with minor modifications.
542 Briefly, K562 cells stably expressing low levels of EGFP-fusion vectors encoding, PCGF1-EGFP, EGFP-
543 RING1B, KDM2B-EGFP or non-transduced K562 cells and CB-MLL-AF9 cells were treated with DMSO
544 or P22077 for indicated timepoints and subsequently cross-linked with 1% formaldehyde for 10 min.
545 Reactions were quenched with addition of Glycine at a final concentration of 125 mM. Cells were
546 lysed in SDS buffer including protease inhibitors (1x CLAP, 0.1 mM PMSF) and snap frozen in liquid

547 nitrogen and stored at -80°C. ChIP was continued by resuspending cells in cold IP buffer and
548 sonicated using a Bioruptor (Diagenode). Pre-clearing was performed by adding Protein G Dynabeads
549 (Invitrogen) and incubated for 15 min at 4°C on a rotating platform. Then ChIP reactions were
550 performed using the following antibodies: anti-GFP (ab290, Abcam), anti-KDM2B (ab137547, Abcam),
551 anti-H2AK119ub (D27C4, Cell Signaling Technology), anti-H3K4me3 (ab8580, Abcam), anti-H3K27ac
552 (C15410196, Diagenode) and IgG (I8141, Sigma) followed by overnight incubation at 4°C on a rotating
553 platform. Next day Protein G Dynabeads were added for 2-4h after beads were separated using a
554 magnetic rack and washed with 3x Mixed Micelle Buffer, 2x Buffer 500, 2x LiCl Detergent Wash
555 Buffer and 1x TE (pH 8.0). ChIP DNA was eluted and reverse cross-linked at 65°C in the presence of
556 1% SDS and 0.1M $NaHCO_3$. Samples were treated with RNase and Proteinase K and purified using
557 QIAquick PCR purification kit (Qiagen). ChIPs were analysed by qPCR as percentage of input, Dataset
558 EV7 lists the qPCR primers used.
559
560 **RNA seq analysis and quantitative real-time PCR**
561 RNA samples for sequencing were prepared for DMSO and P22077 (30 µM) treated K562 cells at 4h,
562 8h, 16h and 24h. Total RNA was isolated using the RNeasy Mini Kit from Qiagen (Venlo, The
563 Netherlands) according to the manufacturer's recommendations. Initial quality check and RNA
564 quantification of the samples was performed by capillary electrophoresis using the LabChip GX
565 (Perkin Elmer). Sequence libraries were generated with 50 ng mRNA, using Lexogen Quantseq 3' prep
566 kit (Lexogen GmbH) according to the manufacturer's recommendations. The obtained cDNA
567 fragment libraries were sequenced on an Illumina NextSeq500 using default parameters (single
568 read). Bioinformatics were performed on the Strand Avadis NGS (v3.0) software (Strand Life Sciences
569 Pvt.Ltd). Sequence quality was checked for GC content, base quality and composition using FASTQC
570 and StrandNGS. Quality trimmed reads were aligned to build Human Hg19 transcriptome. Ensembl
571 Genes and transcripts (2014.01.02) was used as gene annotation database. Quantified reads were

572 normalized using the DESeq package. Reads with failed vendor QC, quality score less than 24
573 (average), mapping quality score below 50 and length less than 20 were all filtered out.
574 For quantitative RT-PCR, RNA was reverse transcribed using the iScript cDNA synthesis kit (Bio-Rad)
575 and amplified using SsoAdvanced SYBR Green Supermix (Bio-Rad) on a CFX384 Touch Real-Time PCR
576 Detection System (Bio-Rad). RPL27 was used as housekeeping gene. Primer sequences are available
577 on request.
578
579 **USP7 inhibition *in vivo***
580 Eight to ten week old female NSG (NOD.Cg-Prkdcscid Il2rgtm1Wjl/SzJ) mice were purchased from the
581 Centrale Dienst Proefdieren (CDP) breeding facility within the University Medical Center Groningen.
582 Mouse experiments were performed in accordance with national and institutional guidelines, and all
583 experiments were approved by the Institutional Animal Care and Use Committee of the University of
584 Groningen (IACUC-RuG). 24h prior to transplantations, mice were sub-lethally irradiated with a dose
585 of 1.0 Gy (X-RAD 320 Unit, PXINC 2010). After irradiation mice received Neomycin (3.5 g/l) in their
586 drinking water and soft food (RM Convalescence + BG SY (M); Special Diet Services; Witham,
587 England) for two weeks. For secondary transplantations, 5 x 10^4 MLL-AF9 EGFP cells from primary
588 leukemic mice (CB MLL-AF9 xenograft mouse model, [49,50]) were injected IV (lateral tail vein).
589 Peripheral blood chimerism levels were monitored by regular blood sample analysis. Mice were
590 randomly divided into two groups, weighted and treated with DMSO as control (n=5) or 20 mg/kg
591 P22077 (n=6) via intraperitoneal (IP) injections daily starting four weeks post-transplant. Prior to
592 injections, P22077 was dissolved in DMSO (or DMSO only as control) and directly mixed with
593 Cremophor EL (1:1). This solution was then diluted 1:4 in saline, to get an end concentration of max.
594 10% DMSO. Mice were humanely terminated by cervical dislocation under isoflurane anesthesia
595 when chimerism levels in the blood exceeded 40%. Peripheral blood, bone marrow, spleen and liver
596 were analysed.
597

598 **Acknowledgements**

599 The authors thank Dr. S. Bergink and E. de Mattos for providing pCl His-Ubi plasmid and advice with
600 ubiquitin experiments. We thank M. Elliot for generation of KDM2B-EGFP construct. We also thank
601 Bart-Jan Wierenga for generation of the pRRL.SFFV.EGFP.miR-E vector. The authors thank FORMA
602 therapeutics (Watertown, MA, USA) for providing the FT671 compound. We would like to thank
603 Roelof-Jan van der Lei, Theo Bijma, Henk Moes en Geert Mesander for help with cell sorting. We
604 acknowledge Prof. Robert E Campbell (Department of Chemistry, University of Alberta, Edmonton,
605 Alberta, Canada) for providing the mBlueberry2 Fluorescent Protein. This work is supported by the
606 European Research Council (ERC-2011-StG 281474-huLSCtargeting) and the Dutch Cancer Foundation
607 (RUG 2014-6832).

608

609 **Conflict of interest**

610 The authors declare no conflict of interests.

611

612 **References**

613 Reference List
614

615 1. Kouzarides T (2007) Chromatin modifications and their function. *Cell* **128:** 693-705
616 2. Simon JA, Kingston RE (2013) Occupying chromatin: Polycomb mechanisms for getting to genomic
617 targets, stopping transcriptional traffic, and staying put. *Mol. Cell* **49:** 808-824
618 3. Mas G, Di CL (2016) The role of Polycomb in stem cell genome architecture. *Curr. Opin. Cell Biol* **43:**
619 87-95
620 4. Boyer LA, Plath K, Zeitlinger J, Brambrink T, Medeiros LA, Lee TI, Levine SS, Wernig M, Tajonar A,
621 Ray MK*, et al.* (2006) Polycomb complexes repress developmental regulators in murine embryonic
622 stem cells. *Nature* **441:** 349-353
623 5. Bracken AP, Dietrich N, Pasini D, Hansen KH, Helin K (2006) Genome-wide mapping of Polycomb
624 target genes unravels their roles in cell fate transitions. *Genes Dev* **20:** 1123-1136
625 6. Lee TI, Jenner RG, Boyer LA, Guenther MG, Levine SS, Kumar RM, Chevalier B, Johnstone SE, Cole
626 MF, Isono K*, et al.* (2006) Control of developmental regulators by Polycomb in human embryonic
627 stem cells. *Cell* **125:** 301-313
628 7. Bracken AP, Helin K (2009) Polycomb group proteins: navigators of lineage pathways led astray in
629 cancer. *Nat. Rev. Cancer* **9:** 773-784
630 8. Hu D, Shilatifard A (2016) Epigenetics of hematopoiesis and hematological malignancies. *Genes*
631 *Dev* **30:** 2021-2041
632 9. Piunti A, Shilatifard A (2016) Epigenetic balance of gene expression by Polycomb and COMPASS
633 families. *Science* **352:** aad9780
634 10. Simon JA, Kingston RE (2009) Mechanisms of polycomb gene silencing: knowns and unknowns.
635 *Nat. Rev. Mol. Cell Biol* **10:** 697-708
636 11. Cao R, Wang L, Wang H, Xia L, Erdjument-Bromage H, Tempst P, Jones RS, Zhang Y (2002) Role of
637 histone H3 lysine 27 methylation in Polycomb-group silencing. *Science* **298:** 1039-1043
638 12. Kuzmichev A, Nishioka K, Erdjument-Bromage H, Tempst P, Reinberg D (2002) Histone
639 methyltransferase activity associated with a human multiprotein complex containing the Enhancer of
640 Zeste protein. *Genes Dev* **16:** 2893-2905
641 13. Kirmizis A, Bartley SM, Kuzmichev A, Margueron R, Reinberg D, Green R, Farnham PJ (2004)
642 Silencing of human polycomb target genes is associated with methylation of histone H3 Lys 27. *Genes*
643 *Dev* **18:** 1592-1605
644 14. Wang H, Wang L, Erdjument-Bromage H, Vidal M, Tempst P, Jones RS, Zhang Y (2004) Role of
645 histone H2A ubiquitination in Polycomb silencing. *Nature* **431:** 873-878
646 15. de Napoles M, Mermoud JE, Wakao R, Tang YA, Endoh M, Appanah R, Nesterova TB, Silva J, Otte
647 AP, Vidal M*, et al.* (2004) Polycomb group proteins Ring1A/B link ubiquitylation of histone H2A to
648 heritable gene silencing and X inactivation. *Dev. Cell* **7:** 663-676
649 16. Gao Z, Zhang J, Bonasio R, Strino F, Sawai A, Parisi F, Kluger Y, Reinberg D (2012) PCGF Homologs,
650 CBX Proteins, and RYBP Define Functionally Distinct PRC1 Family Complexes. *Mol. Cell* **45:** 344-356
651 17. van den Boom V, Maat H, Geugien M, Rodriguez LA, Sotoca AM, Jaques J, Brouwers-Vos AZ,
652 Fusetti F, Groen RW, Yuan H*, et al.* (2016) Non-canonical PRC1.1 Targets Active Genes Independent
653 of H3K27me3 and Is Essential for Leukemogenesis. *Cell Rep* **14:** 332-346
654 18. Wang R, Taylor AB, Leal BZ, Chadwell LV, Ilangovan U, Robinson AK, Schirf V, Hart PJ, Lafer EM,
655 Demeler B*, et al.* (2010) Polycomb group targeting through different binding partners of RING1B C-
656 terminal domain. *Structure* **18:** 966-975
657 19. Cao R, Tsukada Y, Zhang Y (2005) Role of Bmi-1 and Ring1A in H2A ubiquitylation and Hox gene
658 silencing. *Mol. Cell* **20:** 845-854
659 20. Buchwald G, van der Stoop P, Weichenrieder O, Perrakis A, van LM, Sixma TK (2006) Structure
660 and E3-ligase activity of the Ring-Ring complex of polycomb proteins Bmi1 and Ring1b. *EMBO J* **25:**
661 2465-2474

662 21. Elderkin S, Maertens GN, Endoh M, Mallery DL, Morrice N, Koseki H, Peters G, Brockdorff N, Hiom
663 K (2007) A phosphorylated form of Mel-18 targets the Ring1B histone H2A ubiquitin ligase to
664 chromatin. *Mol. Cell* **28:** 107-120
665 22. Rose NR, King HW, Blackledge NP, Fursova NA, Ember KJ, Fischer R, Kessler BM, Klose RJ (2016)
666 RYBP stimulates PRC1 to shape chromatin-based communication between Polycomb repressive
667 complexes. *Elife* **5:**
668 23. van den Boom V, Rozenveld-Geugien M, Bonardi F, Malanga D, van GD, Heijink AM, Viglietto G,
669 Morrone G, Fusetti F, Vellenga E*, et al.* (2013) Non-redundant and locus-specific gene repression
670 functions of PRC1 paralog family members in human hematopoietic stem/progenitor cells. *Blood*
671 **121:** 2452-2461
672 24. Morey L, Santanach A, Blanco E, Aloia L, Nora EP, Bruneau BG, Di CL (2015) Polycomb Regulates
673 Mesoderm Cell Fate-Specification in Embryonic Stem Cells through Activation and Repression
674 Mechanisms. *Cell Stem Cell* **17:** 300-315
675 25. Gearhart MD, Corcoran CM, Wamstad JA, Bardwell VJ (2006) Polycomb group and SCF ubiquitin
676 ligases are found in a novel BCOR complex that is recruited to BCL6 targets. *Mol. Cell Biol* **26:** 6880-
677 6889
678 26. Sanchez C, Sanchez I, Demmers JA, Rodriguez P, Strouboulis J, Vidal M (2007) Proteomics analysis
679 of Ring1B/Rnf2 interactors identifies a novel complex with the Fbxl10/Jhdm1B histone demethylase
680 and the Bcl6 interacting corepressor. *Mol. Cell Proteomics* **6:** 820-834
681 27. He J, Nguyen AT, Zhang Y (2011) KDM2b/JHDM1b, an H3K36me2-specific demethylase, is
682 required for initiation and maintenance of acute myeloid leukemia. *Blood* **117:** 3869-3880
683 28. Andricovich J, Kai Y, Peng W, Foudi A, Tzatsos A (2016) Histone demethylase KDM2B regulates
684 lineage commitment in normal and malignant hematopoiesis. *J. Clin. Invest*, 84014
685 [pii];10.1172/JCI84014 [doi]
686 29. Ueda T, Nagamachi A, Takubo K, Yamasaki N, Matsui H, Kanai A, Nakata Y, Ikeda K, Konuma T,
687 Oda H*, et al.* (2015) Fbxl10 overexpression in murine hematopoietic stem cells induces leukemia
688 involving metabolic activation and upregulation of Nsg2. *Blood*, blood-2014-03-562694
689 [pii];10.1182/blood-2014-03-562694 [doi]
690 30. Kottakis F, Foltopoulou P, Sanidas I, Keller P, Wronski A, Dake BT, Ezell SA, Shen Z, Naber SP,
691 Hinds PW*, et al.* (2014) NDY1/KDM2B Functions as a Master Regulator of Polycomb Complexes and
692 Controls Self-Renewal of Breast Cancer Stem Cells. *Cancer Res* **74:** 3935-3946
693 31. Farcas AM, Blackledge NP, Sudbery I, Long HK, McGouran JF, Rose NR, Lee S, Sims D, Cerase A,
694 Sheahan TW*, et al.* (2012) KDM2B links the Polycomb Repressive Complex 1 (PRC1) to recognition of
695 CpG islands. *Elife* **1:** e00205
696 32. He J, Shen L, Wan M, Taranova O, Wu H, Zhang Y (2013) Kdm2b maintains murine embryonic
697 stem cell status by recruiting PRC1 complex to CpG islands of developmental genes. *Nat. Cell Biol* **15:**
698 373-384
699 33. Blackledge NP, Farcas AM, Kondo T, King HW, McGouran JF, Hanssen LL, Ito S, Cooper S, Kondo K,
700 Koseki Y*, et al.* (2014) Variant PRC1 complex-dependent H2A ubiquitylation drives PRC2 recruitment
701 and polycomb domain formation. *Cell* **157:** 1445-1459
702 34. Wu X, Johansen JV, Helin K (2013) Fbxl10/Kdm2b Recruits Polycomb Repressive Complex 1 to CpG
703 Islands and Regulates H2A Ubiquitylation. *Mol. Cell* **49:** 1134-1146
704 35. Wong SJ, Gearhart MD, Taylor AB, Nanyes DR, Ha DJ, Robinson AK, Artigas JA, Lee OJ, Demeler B,
705 Hart PJ*, et al.* (2016) KDM2B Recruitment of the Polycomb Group Complex, PRC1.1, Requires
706 Cooperation between PCGF1 and BCORL1. *Structure*, S0969-2126(16)30222-2
707 [pii];10.1016/j.str.2016.07.011 [doi]
708 36. Junco SE, Wang R, Gaipa JC, Taylor AB, Schirf V, Gearhart MD, Bardwell VJ, Demeler B, Hart PJ,
709 Kim CA (2013) Structure of the Polycomb Group Protein PCGF1 in Complex with BCOR Reveals Basis
710 for Binding Selectivity of PCGF Homologs. *Structure*, S0969-2126(13)00053-1
711 [pii];10.1016/j.str.2013.02.013 [doi]
712 37. Francis NJ, Kingston RE, Woodcock CL (2004) Chromatin compaction by a polycomb group protein
713 complex. *Science* **306:** 1574-1577

714 38. Muller J, Verrijzer P (2009) Biochemical mechanisms of gene regulation by polycomb group
715 protein complexes. *Curr Opin Genet Dev* **19:** 150-158
716 39. Tzatsos A, Pfau R, Kampranis SC, Tsichlis PN (2009) Ndy1/KDM2B immortalizes mouse embryonic
717 fibroblasts by repressing the Ink4a/Arf locus. *Proc. Natl. Acad. Sci. U. S. A* **106:** 2641-2646
718 40. Boulard M, Edwards JR, Bestor TH (2015) FBXL10 protects Polycomb-bound genes from
719 hypermethylation. *Nat. Genet* **47:** 479-485
720 41. Tavares Λ, Dimitrova E, Oxley D, Webster J, Poot R, Demmers J, Bezstarosti K, Taylor S, Ura H,
721 Koide H*, et al.* (2012) RYBP-PRC1 Complexes Mediate H2A Ubiquitylation at Polycomb Target Sites
722 Independently of PRC2 and H3K27me3. *Cell*,
723 42. Liang G, He J, Zhang Y (2012) Kdm2b promotes induced pluripotent stem cell generation by
724 facilitating gene activation early in reprogramming. *Nat. Cell Biol* **14:** 457-466
725 43. Engelen E, Brandsma JH, Moen MJ, Signorile L, Dekkers DH, Demmers J, Kockx CE, Ozgur Z, van
726 IJcken WF, van den Berg DL*, et al.* (2015) Proteins that bind regulatory regions identified by histone
727 modification chromatin immunoprecipitations and mass spectrometry. *Nat. Commun* **6:** 7155
728 44. Leznicki P, Kulathu Y (2017) Mechanisms of regulation and diversification of deubiquitylating
729 enzyme function. *J Cell Sci* **130:** 1997-2006
730 45. Tian X, Isamiddinova NS, Peroutka RJ, Goldenberg SJ, Mattern MR, Nicholson B, Leach C (2011)
731 Characterization of selective ubiquitin and ubiquitin-like protease inhibitors using a fluorescence-
732 based multiplex assay format. *Assay Drug Dev Technol* **9:** 165-173
733 46. Altun M, Kramer HB, Willems LI, McDermott JL, Leach CA, Goldenberg SJ, Kumar KG, Konietzny R,
734 Fischer R, Kogan E*, et al.* (2011) Activity-based chemical proteomics accelerates inhibitor
735 development for deubiquitylating enzymes. *Chem Biol* **18:** 1401-1412
736 47. Turnbull AP, Ioannidis S, Krajewski WW, Pinto-Fernandez A, Heride C, Martin ACL, Tonkin LM,
737 Townsend EC, Buker SM, Lancia DR*, et al.* (2017) Molecular basis of USP7 inhibition by selective
738 small-molecule inhibitors. *Nature*, 10.1038/nature24451
739 48. Li M, Brooks CL, Kon N, Gu W (2004) A dynamic role of HAUSP in the p53-Mdm2 pathway. *Mol*
740 *Cell* **13:** 879-886
741 49. Horton SJ, Jaques J, Woolthuis C, van DJ, Mesuraca M, Huls G, Morrone G, Vellenga E, Schuringa
742 JJ (2013) MLL-AF9-mediated immortalization of human hematopoietic cells along different lineages
743 changes during ontogeny. *Leukemia* **27:** 1116-1126
744 50. Sontakke P, Carretta M, Jaques J, Brouwers-Vos AZ, Lubbers-Aalders L, Yuan H, de Bruijn JD,
745 Martens AC, Vellenga E, Groen RW*, et al.* (2016) Modeling BCR-ABL and MLL-AF9 leukemia in a
746 human bone marrow-like scaffold-based xenograft model. *Leukemia* **30:** 2064-2073
747 51. Karjalainen R, Pemovska T, Popa M, Liu M, Javarappa KK, Majumder MM, Yadav B, Tamborero D,
748 Tang J, Bychkov D*, et al.* (2017) JAK1/2 and BCL2 inhibitors synergize to counteract bone marrow
749 stromal cell-induced protection of AML. *Blood* **130:** 789-802
750 52. Greim H, Kaden DA, Larson RA, Palermo CM, Rice JM, Ross D, Snyder R (2014) The bone marrow
751 niche, stem cells, and leukemia: impact of drugs, chemicals, and the environment. *Ann. N. Y. Acad.*
752 *Sci* **1310:** 7-31
753 53. Parmar A, Marz S, Rushton S, Holzwarth C, Lind K, Kayser S, Dohner K, Peschel C, Oostendorp RA,
754 Gotze KS (2011) Stromal niche cells protect early leukemic FLT3-ITD+ progenitor cells against first-
755 generation FLT3 tyrosine kinase inhibitors. *Cancer Res* **71:** 4696-4706
756 54. Taherbhoy AM, Huang OW, Cochran AG (2015) BMI1-RING1B is an autoinhibited RING E3
757 ubiquitin ligase. *Nat. Commun* **6:** 7621
758 55. Endoh M, Endo TA, Endoh T, Fujimura Y, Ohara O, Toyoda T, Otte AP, Okano M, Brockdorff N,
759 Vidal M*, et al.* (2008) Polycomb group proteins Ring1A/B are functionally linked to the core
760 transcriptional regulatory circuitry to maintain ES cell identity. *Development* **135:** 1513-1524
761 56. Dou H, Buetow L, Sibbet GJ, Cameron K, Huang DT (2012) BIRC7-E2 ubiquitin conjugate structure
762 reveals the mechanism of ubiquitin transfer by a RING dimer. *Nat Struct Mol Biol* **19:** 876-883
763 57. Lecona E, Narendra V, Reinberg D (2015) USP7 COOPERATES WITH SCML2 TO REGULATE THE
764 ACTIVITY OF PRC1. *Mol. Cell Biol*, MCB.01197-14 [pii];10.1128/MCB.01197-14 [doi]

765 58. Maertens GN, El Messaoudi-Aubert S, Elderkin S, Hiom K, Peters G (2010) Ubiquitin-specific
766 proteases 7 and 11 modulate Polycomb regulation of the INK4a tumour suppressor. *Embo j* **29:** 2553-
767 2565
768 59. Ning B, Zhao W, Qian C, Liu P, Li Q, Li W, Wang RF (2017) USP26 functions as a negative regulator
769 of cellular reprogramming by stabilising PRC1 complex components. *Nat. Commun* **8:** 349
770 60. de BP, Zaaroor-Regev D, Ciechanover A (2010) Regulation of the Polycomb protein RING1B
771 ubiquitination by USP7. *Biochem. Biophys. Res. Commun* **400:** 389-395
772 61. Ben-Saadon R, Zaaroor D, Ziv T, Ciechanover A (2006) The polycomb protein Ring1B generates
773 self atypical mixed ubiquitin chains required for its in vitro histone H2A ligase activity. *Mol Cell* **24:**
774 701-711
775 62. van der Knaap JA, Kumar BR, Moshkin YM, Langenberg K, Krijgsveld J, Heck AJ, Karch F, Verrijzer
776 CP (2005) GMP synthetase stimulates histone H2B deubiquitylation by the epigenetic silencer USP7.
777 *Mol Cell* **17:** 695-707
778 63. Sarkari F, Sanchez-Alcaraz T, Wang S, Holowaty MN, Sheng Y, Frappier L (2009) EBNA1-mediated
779 recruitment of a histone H2B deubiquitylating complex to the Epstein-Barr virus latent origin of DNA
780 replication. *PLoS Pathog* **5:** e1000624
781 64. Lee JH, Skalnik DG (2005) CpG-binding protein (CXXC finger protein 1) is a component of the
782 mammalian Set1 histone H3-Lys4 methyltransferase complex, the analogue of the yeast
783 Set1/COMPASS complex. *J Biol Chem* **280:** 41725-41731
784 65. Antonelli A, Noort WA, Jaques J, de BB, de Jong-Korlaar R, Brouwers-Vos AZ, Lubbers-Aalders L,
785 van Velzen JF, Bloem AC, Yuan H*, et al.* (2016) Establishing human leukemia xenograft mouse models
786 by implanting human bone marrow-like scaffold-based niches. *Blood* **128:** 2949-2959
787 66. Kategaya L, Di Lello P, Rouge L, Pastor R, Clark KR, Drummond J, Kleinheinz T, Lin E, Upton JP,
788 Prakash S*, et al.* (2017) USP7 small-molecule inhibitors interfere with ubiquitin binding. *Nature*,
789 10.1038/nature24006
790 67. Carra G, Panuzzo C, Torti D, Parvis G, Crivellaro S, Familiari U, Volante M, Morena D, Lingua MF,
791 Brancaccio M*, et al.* (2017) Therapeutic inhibition of USP7-PTEN network in chronic lymphocytic
792 leukemia: a strategy to overcome TP53 mutated/deleted clones. *Oncotarget* **8:** 35508-35522
793 68. Felle M, Joppien S, Nemeth A, Diermeier S, Thalhammer V, Dobner T, Kremmer E, Kappler R,
794 Langst G (2011) The USP7/Dnmt1 complex stimulates the DNA methylation activity of Dnmt1 and
795 regulates the stability of UHRF1. *Nucleic Acids Res* **39:** 8355-8365
796 69. van der Horst A, de Vries-Smits AM, Brenkman AB, van Triest MH, van den Broek N, Colland F,
797 Maurice MM, Burgering BM (2006) FOXO4 transcriptional activity is regulated by monoubiquitination
798 and USP7/HAUSP. *Nature cell biology* **8:** 1064-1073
799 70. Fan YH, Cheng J, Vasudevan SA, Dou J, Zhang H, Patel RH, Ma IT, Rojas Y, Zhao Y, Yu Y*, et al.*
800 (2013) USP7 inhibitor P22077 inhibits neuroblastoma growth via inducing p53-mediated apoptosis.
801 *Cell Death Dis* **4:** e867
802 71. Ye M, Tang Y, Tang S, Liu J, Wu K, Yao S, Sun Y, Zhou L, Deng T, Chen Y*, et al.* (2015) STIP is a
803 critical nuclear scaffolding protein linking USP7 to p53-Mdm2 pathway regulation. *Oncotarget* **6:**
804 34718-34731
805 72. Colland F, Formstecher E, Jacq X, Reverdy C, Planquette C, Conrath S, Trouplin V, Bianchi J,
806 Aushev VN, Camonis J*, et al.* (2009) Small-molecule inhibitor of USP7/HAUSP ubiquitin protease
807 stabilizes and activates p53 in cells. *Mol Cancer Ther* **8:** 2286-2295
808 73. Hu M, Gu L, Li M, Jeffrey PD, Gu W, Shi Y (2006) Structural basis of competitive recognition of p53
809 and MDM2 by HAUSP/USP7: implications for the regulation of the p53-MDM2 pathway. *PLoS Biol* **4:**
810 e27
811 74. Kon N, Kobayashi Y, Li M, Brooks CL, Ludwig T, Gu W (2010) Inactivation of HAUSP in vivo
812 modulates p53 function. *Oncogene* **29:** 1270-1279
813 75. Tavana O, Li D, Dai C, Lopez G, Banerjee D, Kon N, Chen C, Califano A, Yamashiro DJ, Sun H*, et al.*
814 (2016) HAUSP deubiquitinates and stabilizes N-Myc in neuroblastoma. *Nat Med* **22:** 1180-1186
815 76. Cox J, Mann M (2008) MaxQuant enables high peptide identification rates, individualized p.p.b.-
816 range mass accuracies and proteome-wide protein quantification. *Nat. Biotechnol* **26:** 1367-1372

817 77. Tyanova S, Temu T, Sinitcyn P, Carlson A, Hein MY, Geiger T, Mann M, Cox J (2016) The Perseus
818 computational platform for comprehensive analysis of (prote)omics data. *Nat. Methods* **13:** 731-740
819 78. Fellmann C, Hoffmann T, Sridhar V, Hopfgartner B, Muhar M, Roth M, Lai DY, Barbosa IA, Kwon
820 JS, Guan Y*, et al.* (2013) An Optimized microRNA Backbone for Effective Single-Copy RNAi. *Cell Rep* **5:**
821 1704-1713
822 79. van Gosliga D, Schepers H, Rizo A, van der Kolk D, Vellenga E, Schuringa JJ (2007) Establishing
823 long-term cultures with self-renewing acute myeloid leukemia stem/progenitor cells. *Exp. Hematol*
824 **35:** 1538-1549

825

826

827

828 **Figure legends**

829

830 **Figure 1. The deubiquitinase USP7 interacts with non-canonical PRC1.1 proteins**

831 (A) Visualization of KDM2B interactome using Cytoscape, categorized by Molecular Function as

832 annotated by DAVID.

833 (B) Gene Ontology analysis of KDM2B interactome shown as Biological Process.

834 (C) Schematic representation of the non-canonical PRC1.1 complex, including USP7. PRC1.1

835 preferentially binds to non-methylated CpG islands via the ZF-CxxC domain of KDM2B. The

836 ubiquitination of histone H2A on lysine 119 is mediated by RING1A/B. PRC1.1 can be recruited to

837 active genes in leukemic cells, indicated by H3K4me3.

838 (D) Identification of USP7 and other PRC1.1 proteins by LC-MS/MS in KDM2B-EGFP, PCGF1-EGFP and

839 EGFP-RING1B pull outs from nuclear extracts in K562 cells. The numbers indicate MS/MS counts for

840 each interacting protein corrected for expected peptides based on *in silico* digests (x10).

841 (E) Validation of USP7 and RING1B interactions as analysed by Western blot in canonical PRC1

842 (PCGF2/PCGF4/CBX2/RING1B) and non-canonical PRC1.1 (PCGF1/RING1B) pull outs. Input (I), non-

843 bound (NB) and bound (B) fractions are shown.

844

845 **Figure 2. USP7 deubiquitinase activity is essential for PRC1.1 integrity**

846 (A) Purification of his-tagged ubiquitinated proteins under denaturing conditions in EGFP-RING1B and
847 PCGF1-EGFP cells treated with DMSO (-) or P22077 (+) for 24h followed by Western blot analysis.

848 (B) Label-free quantification (LFQ) intensities of EGFP pull outs on EGFP-RING1B (left) and PCGF1-
849 EGFP (right) interactions, performed in technical replicates in control (DMSO, 0.1%) and USP7i
850 treated cells are illustrated as Volcano plot. The fold change difference (log2) of the EGFP pull out in
851 control versus USP7i is plotted against the –log10 t-test p-value (y-axis). The bait protein
852 (RING1B/PCGF1) is highlighted in green, PRC1.1 proteins in orange and UBB protein in purple.

853 (C) Intensity based absolute quantification (iBAQ) values for several identified PRC1.1 proteins are
854 shown in USP7i/control EGFP pull outs relative to RING1B (left) and PCGF1 (right). Data are shown as
855 mean ± SD (n=2 or 3).

856 (D) Western blot of EGFP pull outs on PCGF1-EGFP and EGFP-RING1B in the absence (-) or presence
857 (+) of P22077 for 72h probed with antibodies for EGFP, RING1B and PCGF1. Input (I), non-bound (NB)
858 and bound (B) fractions are shown.

859 (E) Mean fluorescent intensity (MFI) analysis of EGFP-RING1B and PCGF1-EGFP K562 cells in control
860 or USP7i treated cells at 72h.

861

862 **Figure 3. Loss of PRC1.1 occupancy and H2AK119ub at target loci upon USP7 inhibition**

863 (A) ChIP-qPCRs on control or 72h P22077 (USP7i) treated K562 cells for endogenous KDM2B, PCGF1-

864 EGFP, EGFP-RING1B (B) H2AK119ub and (C) H3K4me3 on several PRC1.1 loci previously identified by

865 ChIP-seq. Error bars represent SD of technical qPCR replicates.

866 (D) ChIP-qPCRs on control or USP7i treated K562 cells for 4h/8h/16h (▬) for H2AK119ub, KDM2B-

867 EGFP, EGFP-RING1B and (E) H3K27ac on four PRC1.1 loci. Error bars represent SD of technical qPCR

868 replicates.

869 (F) ChIP-qPCRs on control or 24h FT671 (10 µM) treated K562 cells for endogenous KDM2B and

870 H2AK119ub. Error bars represent SD of technical qPCR replicates.

871

872 **Figure 4. USP7 inhibition leads to downregulation of a subset of PRC1.1 active target genes**

873 (A) Venn diagram showing overlap of genes downregulated by more than two fold after 24h of USP7
874 inhibition with previously identified PRC1.1 target genes. Gene Ontology analysis of downregulated
875 genes identified as PRC1.1 targets (73) or Polycomb independent targets (224) shown as Biological
876 Process.

877 (B) ChIP-seq profiles of TOP2B, SIN3A, CHD1 and MYC as representative examples for PRC1.1 target
878 genes (73). Our ChIP-seq tracks are shown for GFP (control), H2AK119ub, H3K27me3, PCGF1, PCGF2,
879 PCGF4, CBX2, RING1A, RING1B and KDM2B. ChIP-seq tracks for H3K4me3, H3K36me3, RNAPII and
880 H3K27ac were downloaded from ENCODE/Broad.

881 (C) ChIP-qPCRs in control or 72h USP7i for KDM2B, PCGF1-EGFP, EGFP-RING1B and H2AK119ub or
882 16h USP7i for H3K4me3 and H3K27ac. Error bars represent SD of technical qPCR replicates.

883 (D) Validation of relative gene expression levels of PRC1.1 target genes by qRT-PCR in control and
884 P22077 treated cells (24h). Data are represented as mean ± SD.

885

886 **Figure 5: Sensitiviy of primary AMLs towards USP7 inhibition**

887 (A) Cumulative cell growth of various AML cell lines in control (DMSO) or P22077 treated (5, 10 and
888 20 µM) conditions.

889 (B) Cumulative cell growth of various AML cell lines exposed to different concentrations of the USP7
890 inhibitor FT671, performed in duplicate.

891 (C) Cumulative cell growth of primary AML patient cells (n=3) grown on MS5 co-culture treated with
892 DMSO (control) or P22077 (20 µM) performed in duplicate.

893 (D) Analysis of both cycling and quiescent AML cells by Hoechst/PyroninY stainings within the
894 $CD34^+/CD38^+$ and $CD34^+/CD38^-$ populations (E) or whole population (AML3). Cells were treated with
895 DMSO (control) or P22077 (20 µM) for 3 days while AMLs were grown on MS5 co-culture. Absolute
896 cell numbers were calculated in G_0, G_1 and $S/G_2/M$ fractions.

897

898 **Figure 6: Evaluation of USP7 inhibition in xenograft leukemia mouse model**

899 (A) Experimental setup of our human CB MLL-AF9 xenograft mouse model. Here 5 x 10^4 MLL-AF9
900 EGFP cells from a primary leukemic mouse were IV injected into secondary recipients (n=11).

901 (B) Peripheral blood analysis of MLL-AF9 EGFP/$CD45^+$/$CD19^+$ cells, three weeks after injection prior to
902 treatment (left) and 2.5 weeks following treatment (right). Mice were treated daily with either DMSO
903 as control (n=5) or 20 mg/kg P22077 (n=6).

904 (C) Peripheral blood chimerism levels of control and P22077 (20 mg/kg) treated mice over the course
905 of the experiment. Treatment was started at day 28 (4 weeks post-transplant) indicated with the
906 arrow.

907 (D) Kaplan-Meier curve showing the survival of DMSO (n=5) and P22077 (n=6) treated mice.
908 Statistical analysis was performed using a log-rank test.

909 (E) Cumulative cell growth of CB MLL-AF9 cells grown under myeloid permissive conditions in liquid
910 and co-culture on MS5, treated with DMSO (control) or P22077 (15 and 20 µM). Error bars represent
911 standard deviation of two independent experiments.

912 (F) ChIP-qPCR for KDM2B in CB MLL-AF9 cells treated with DMSO or P22077 (48h) under either liquid
913 culture or MS5 co-culture conditions. Error bars represent SD of technical qPCR replicates.

914

915

916 **Expanded View Figure legends**

917

918 **Figure EV1: Stability of protein expression upon USP7 inhibition**

919 (A) Mean fluorescent intensity (MFI) analysis of EGFP-RING1B and PCGF1-EGFP K562 cells in control

920 or USP7i treated cells for 4 days and (B) of KDM2B-EGFP K562 cells in control or USP7i treated cells

921 for 3 days.

922

923 **Figure EV2: Evaluation of USP7 knockdown on KDM2B binding**

924 (A) USP7 knockdown efficiencies validated by qPCR, 3 days after transductions in K562 cells.

925 (B) KDM2B ChIP in K562 miR-E SCR and miR-E USP7#A and #B transduced cells, 3 days after

926 transduction. qPCRs were performed on several PRC1.1 target loci. Error bars represent SD of

927 technical qPCR replicates.

928

929 **Figure EV3: Sensitivity of lymphoid MLL-AF9 cells grown on MS5 for P22077**

930 (A) Lymphoid MLL-AF9 (GFP) co-culture on murine stromal cells treated with DMSO or P22077 (20

931 µM), day 6. Lymphoid MLL-AF9 cells typically form cobblestone areas (left). Absolute cell numbers

932 corrected for human $CD45^+$ and GFP^+ are shown 10 days upon DMSO or P22077 (20 µm) treatment

933 (right).

934

Fig 1

A

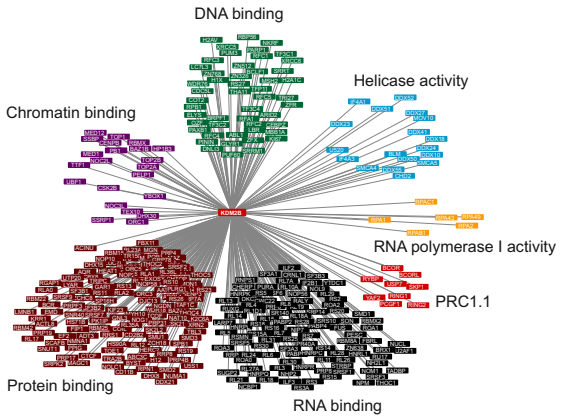

B

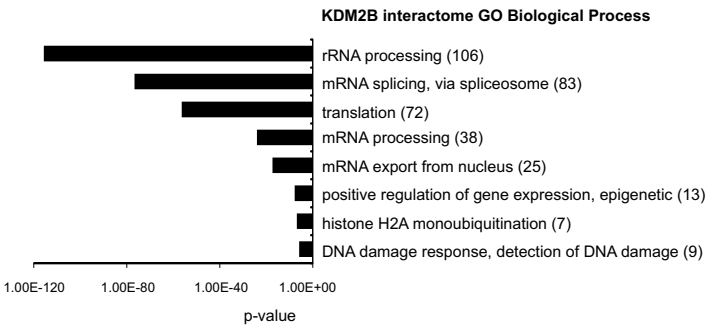

C

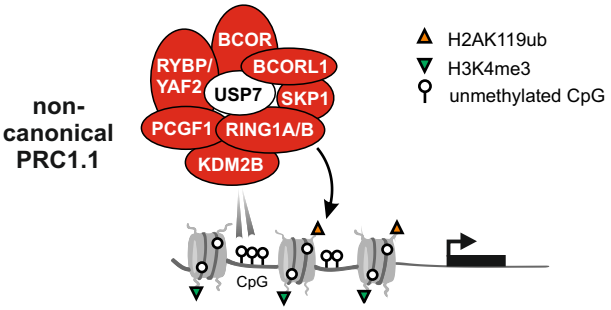

D

	KDM2B	PCGF1	RING1B
USP7	25	30	19
PCGF1	40	91	25
BCOR	12	19	11
BCORL1	9	13	13
KDM2B	131	19	16
SKP1	98	10	4
RYBP	10	19	11
YAF2	9	19	25
RING1A	35	84	0
RING1B	18	39	166

MS/MS counts corrected (x10)

E

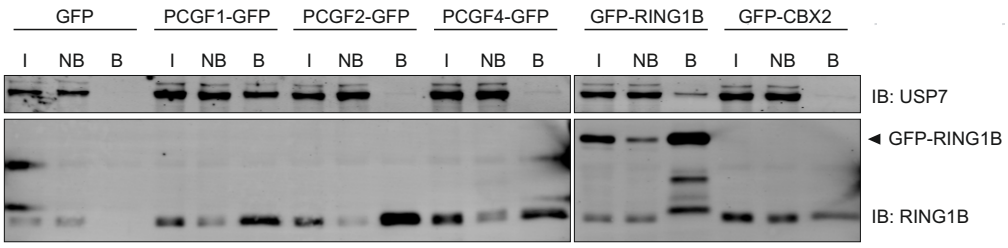

Fig 2

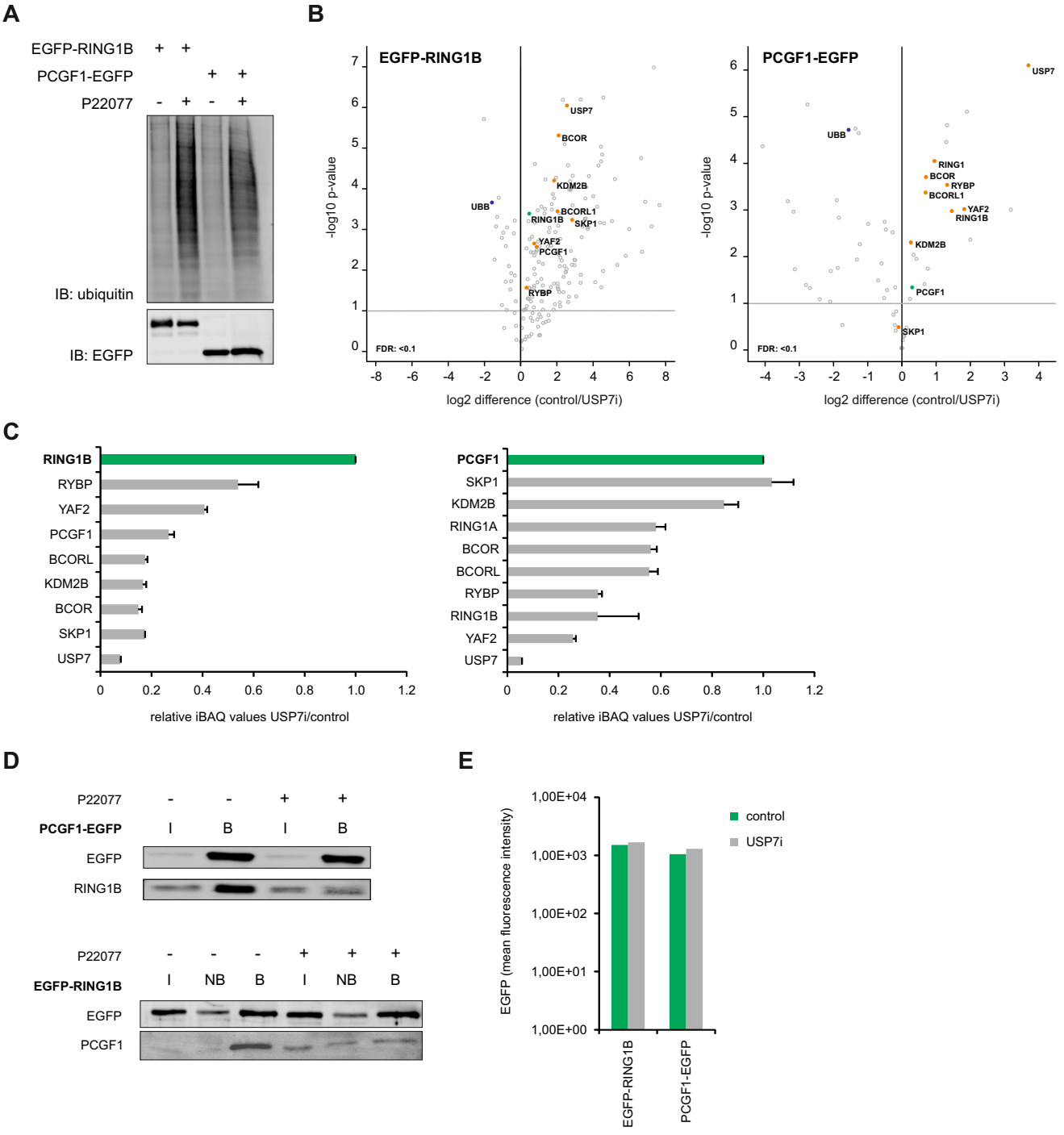
A
EGFP-RING1B + +
PCGF1-EGFP + +
P22077 - + - +
IB: ubiquitin
IB: EGFP
B
EGFP-RING1B
-log10 p-value
log2 difference (control/USP7i)
FDR: <0.1
USP7
BCOR
KDM2B
UBB
BCORL1
RING1B
SKP1
YAF2
PCGF1
RYBP
PCGF1-EGFP
RING1
C
RING1B
RYBP
YAF2
PCGF1
BCORL
KDM2B
BCOR
SKP1
USP7
relative iBAQ values USP7i/control
PCGF1
SKP1
KDM2B
RING1A
BCOR
BCORL
RYBP
RING1B
YAF2
USP7
relative iBAQ values USP7i/control
D
P22077 - - + +
PCGF1-EGFP I B I B
EGFP
RING1B
P22077 - - - + + +
EGFP-RING1B I NB B I NB B
EGFP
PCGF1
E
EGFP (mean fluorescence intensity)
1,00E+04
1,00E+03
1,00E+02
1,00E+01
1,00E+00
control
USP7i
EGFP-RING1B
PCGF1-EGFP

Fig 3

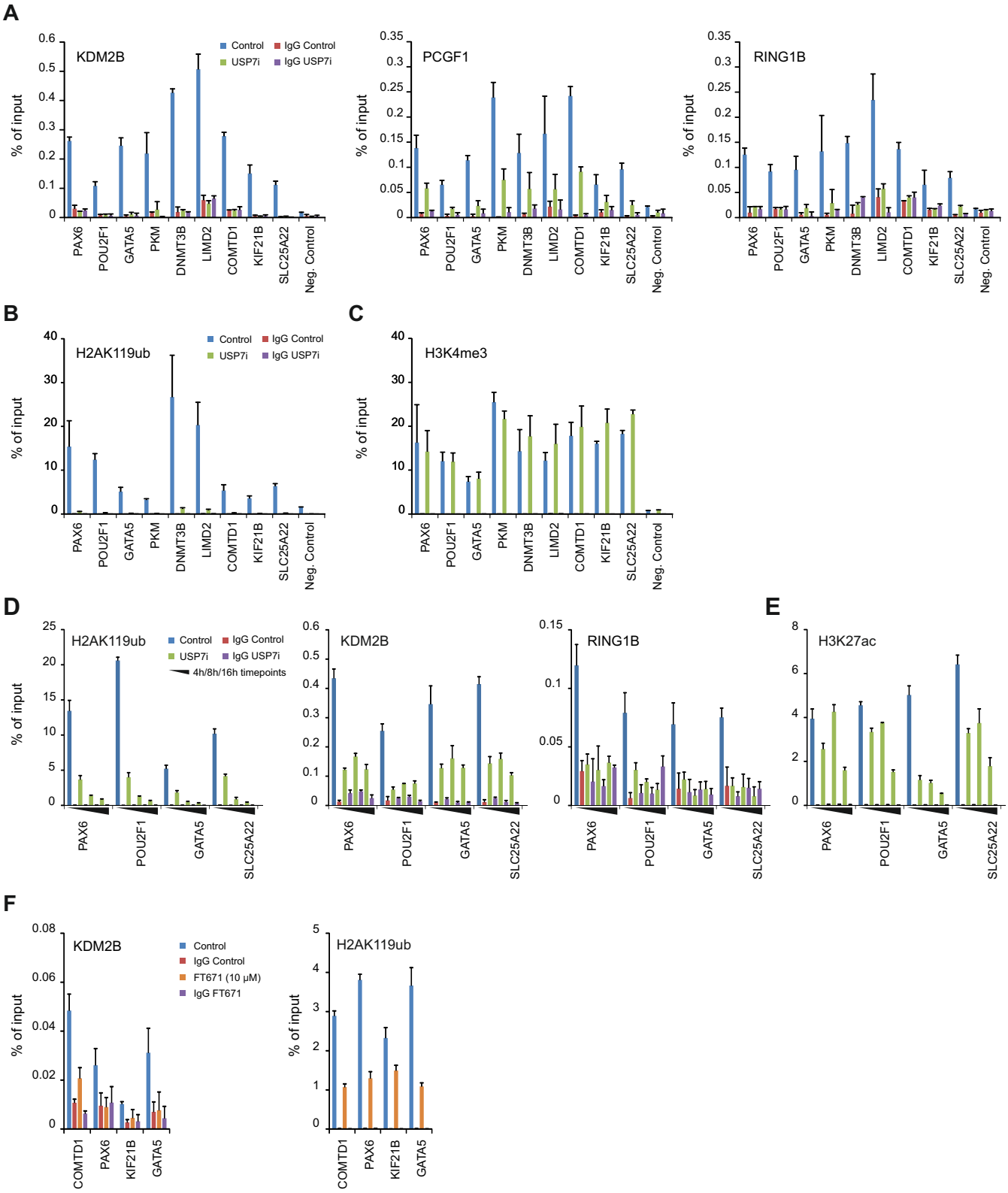
A
KDM2B
PCGF1
RING1B
Control
IgG Control
USP7i
IgG USP7i
% of input
PAX6
POU2F1
GATA5
PKM
DNMT3B
LIMD2
COMTD1
KIF21B
SLC25A22
Neg. Control
B
H2AK119ub
C
H3K4me3
D
H2AK119ub
KDM2B
RING1B
4h/8h/16h timepoints
E
H3K27ac
F
KDM2B
H2AK119ub
Control
IgG Control
FT671 (10 μM)
IgG FT671

Fig 4

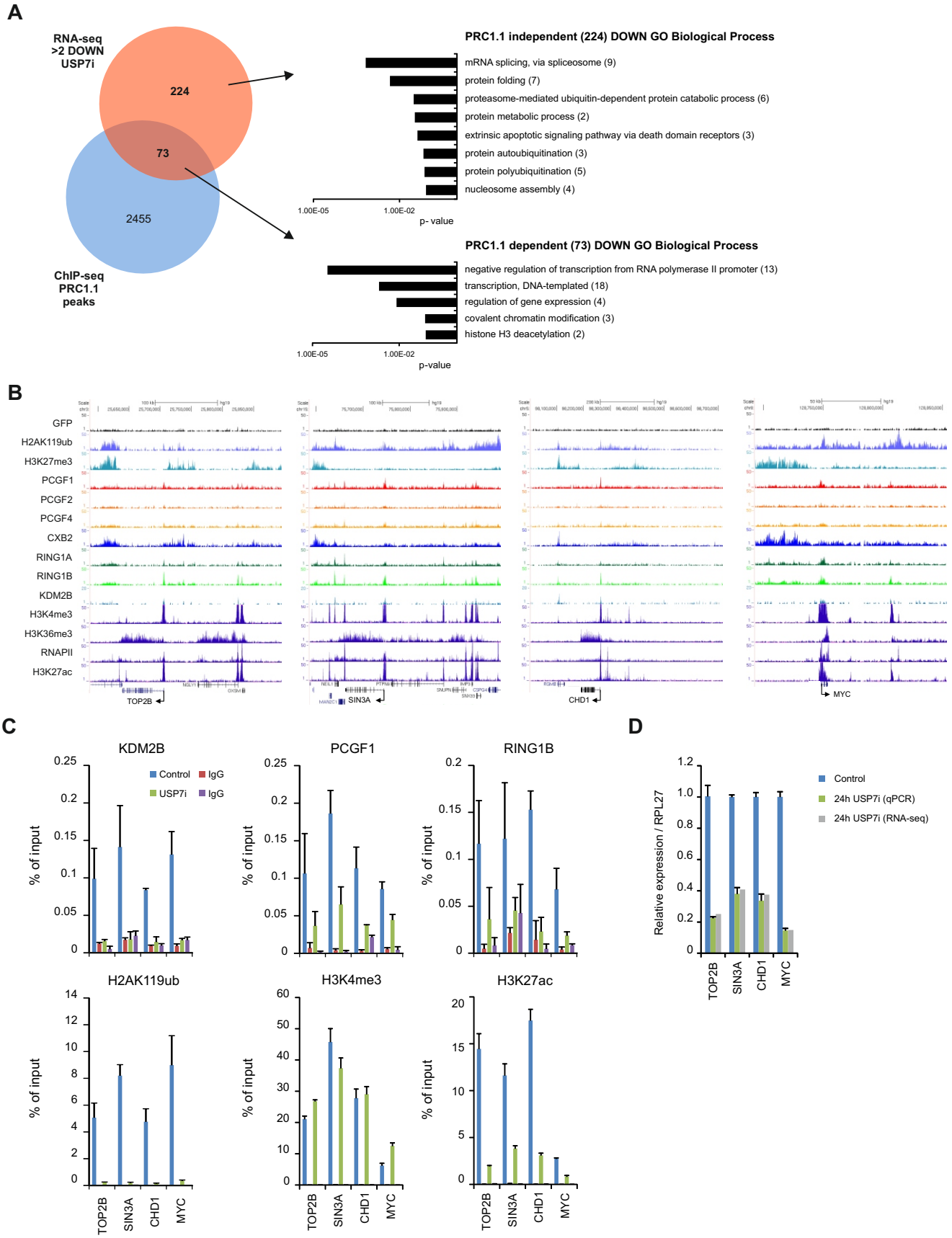
A
RNA-seq
>2 DOWN
USP7i
224
73
2455
ChIP-seq
PRC1.1
peaks
PRC1.1 independent (224) DOWN GO Biological Process
mRNA splicing, via spliceosome (9)
protein folding (7)
proteasome-mediated ubiquitin-dependent protein catabolic process (6)
protein metabolic process (2)
extrinsic apoptotic signaling pathway via death domain receptors (3)
protein autoubiquitination (3)
protein polyubiquitination (5)
nucleosome assembly (4)
1.00E-05
1.00E-02
p- value
PRC1.1 dependent (73) DOWN GO Biological Process
negative regulation of transcription from RNA polymerase II promoter (13)
transcription, DNA-templated (18)
regulation of gene expression (4)
covalent chromatin modification (3)
histone H3 deacetylation (2)
1.00E-05
1.00E-02
p-value
B
GFP
H2AK119ub
H3K27me3
PCGF1
PCGF2
PCGF4
CXB2
RING1A
RING1B
KDM2B
H3K4me3
H3K36me3
RNAPII
H3K27ac
TOP2B
SIN3A
CHD1
MYC
C
KDM2B
PCGF1
RING1B
H2AK119ub
H3K4me3
H3K27ac
Control
IgG
USP7i
IgG
% of input
TOP2B
SIN3A
CHD1
MYC
D
Relative expression / RPL27
Control
24h USP7i (qPCR)
24h USP7i (RNA-seq)
TOP2B
SIN3A
CHD1
MYC

Fig 5

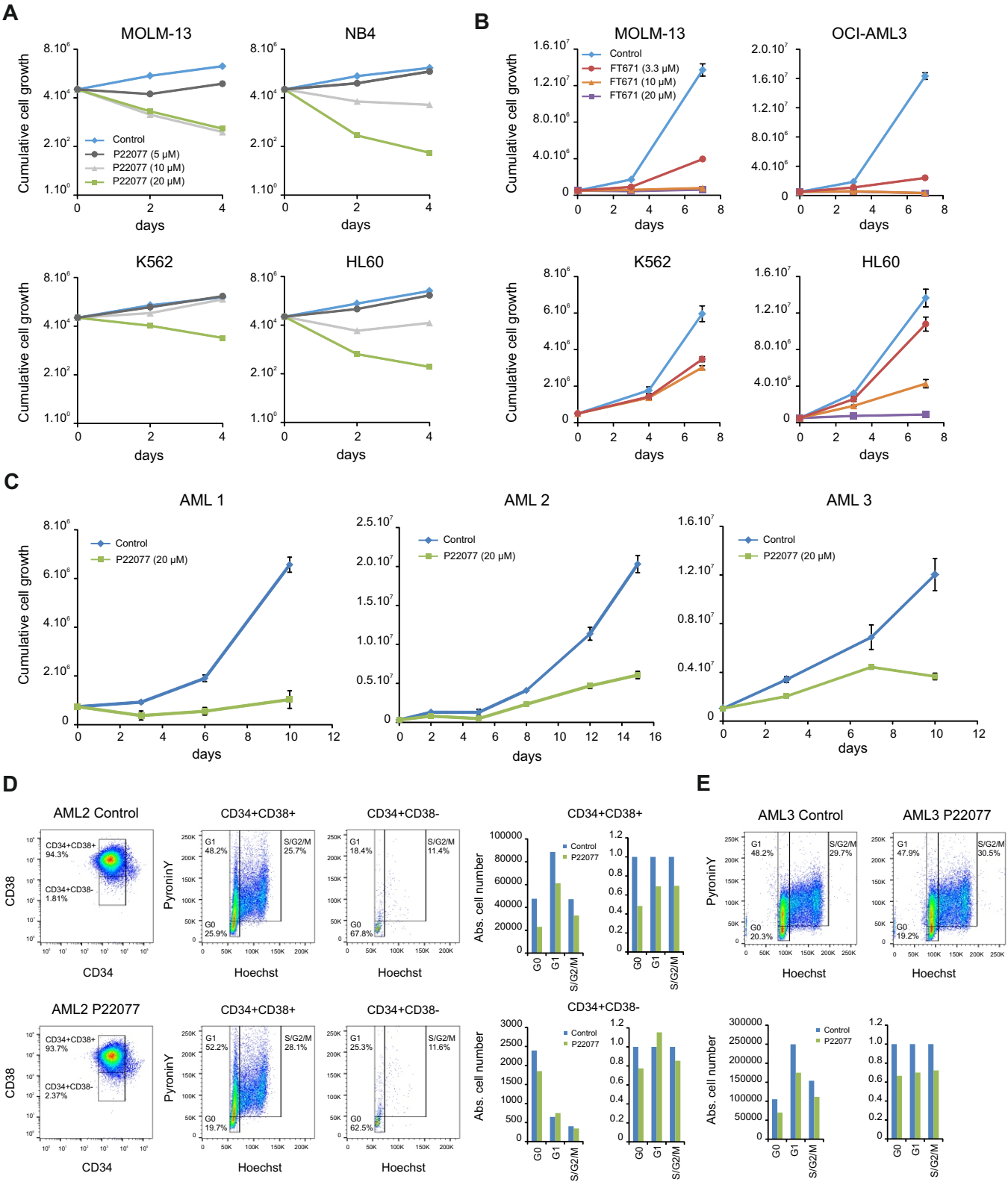
A
MOLM-13
NB4
K562
HL60
Cumulative cell growth
days
Control
P22077 (5 µM)
P22077 (10 µM)
P22077 (20 µM)
B
MOLM-13
OCI-AML3
K562
HL60
Control
FT671 (3.3 µM)
FT671 (10 µM)
FT671 (20 µM)
C
AML 1
AML 2
AML 3
Control
P22077 (20 µM)
D
AML2 Control
AML2 P22077
CD34+CD38+
CD34+CD38-
CD38
CD34
Pyronin Y
Hoechst
Abs. cell number
G0
G1
S/G2/M
E
AML3 Control
AML3 P22077

Fig 6

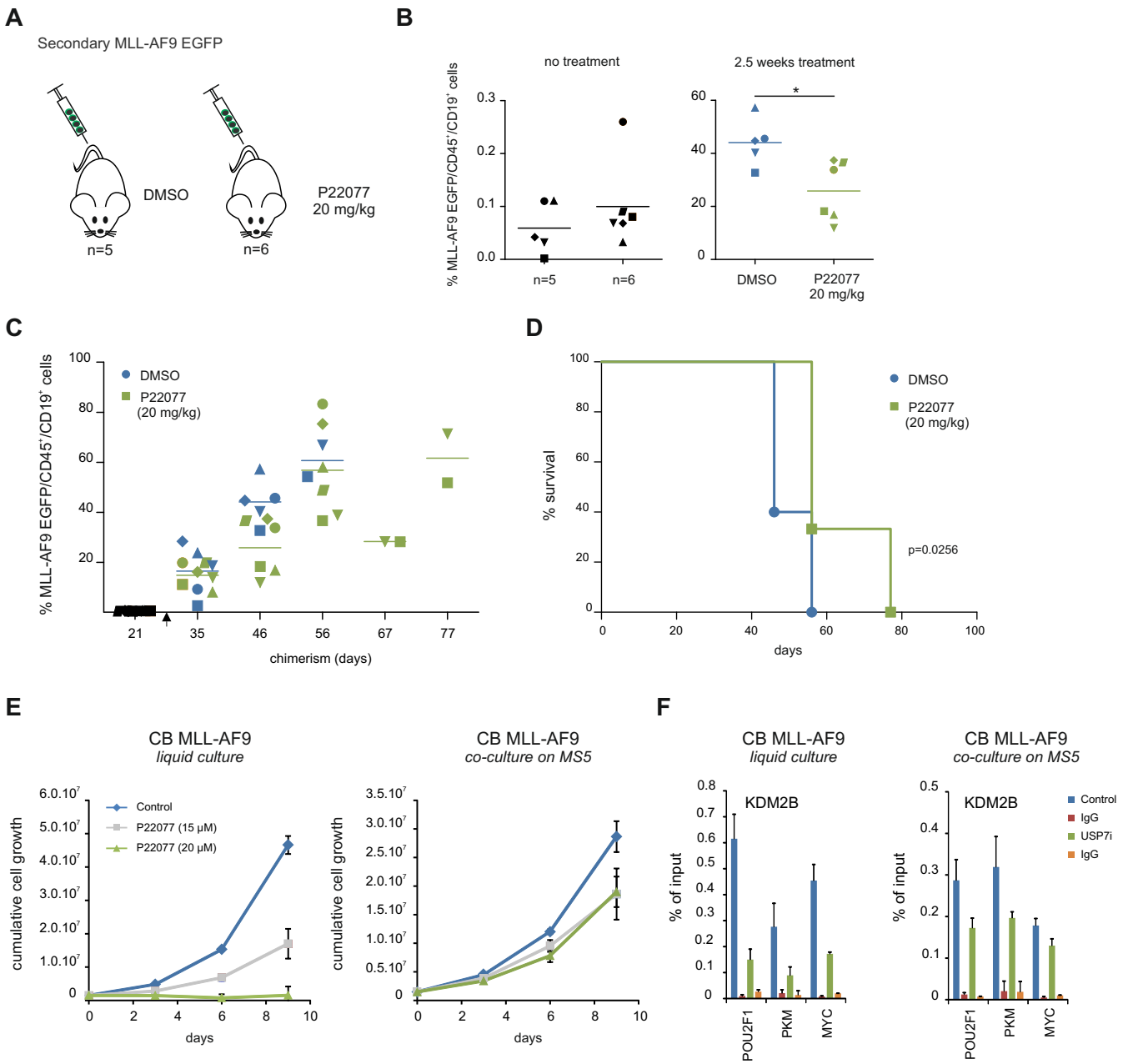
A
Secondary MLL-AF9 EGFP
DMSO
n=5
P22077
20 mg/kg
n=6
B
no treatment
2.5 weeks treatment
% MLL-AF9 EGFP/CD45⁻/CD19⁺ cells
n=5
n=6
DMSO
P22077
20 mg/kg
*
C
% MLL-AF9 EGFP/CD45⁻/CD19⁺ cells
DMSO
P22077
(20 mg/kg)
chimerism (days)
D
% survival
DMSO
P22077
(20 mg/kg)
p=0.0256
days
E
CB MLL-AF9
liquid culture
cumulative cell growth
Control
P22077 (15 μM)
P22077 (20 μM)
days
CB MLL-AF9
co-culture on MS5
cumulative cell growth
days
F
CB MLL-AF9
liquid culture
KDM2B
% of input
POU2F1
PKM
MYC
CB MLL-AF9
co-culture on MS5
KDM2B
Control
IgG
USP7i
IgG
% of input
POU2F1
PKM
MYC

Fig EV1

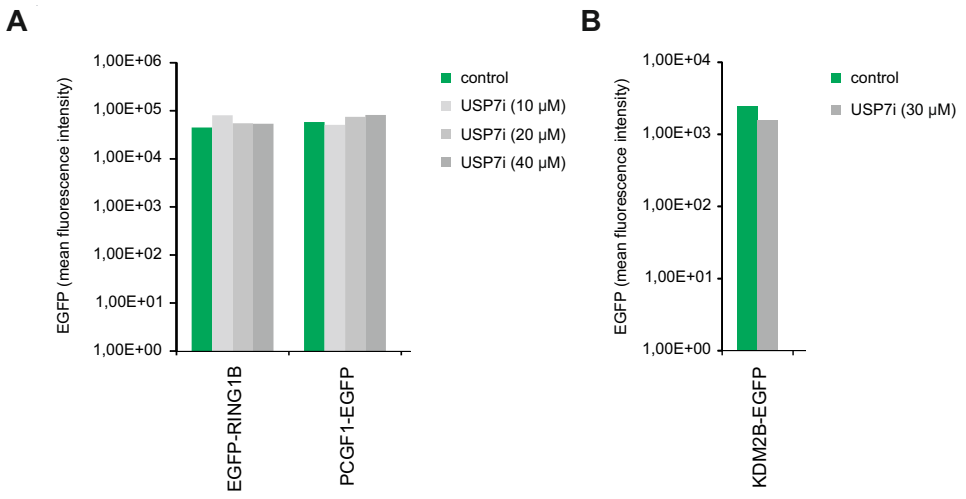
A
EGFP (mean fluorescence intensity)
1,00E+06
1,00E+05
1,00E+04
1,00E+03
1,00E+02
1,00E+01
1,00E+00
EGFP-RING1B
PCGF1-EGFP
control
USP7i (10 μM)
USP7i (20 μM)
USP7i (40 μM)
B
EGFP (mean fluorescence intensity)
1,00E+04
1,00E+03
1,00E+02
1,00E+01
1,00E+00
KDM2B-EGFP
control
USP7i (30 μM)

Fig EV2

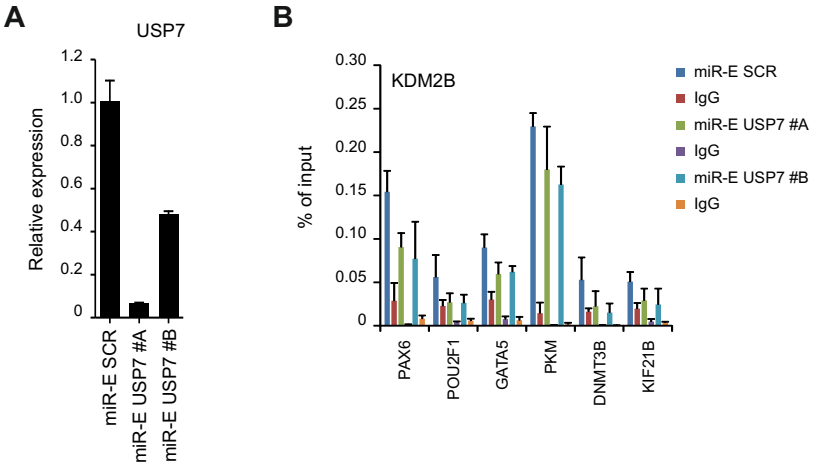
A
USP7
Relative expression
1.2
1.0
0.8
0.6
0.4
0.2
0
miR-E SCR
miR-E USP7 #A
miR-E USP7 #B
B
KDM2B
% of input
0.30
0.25
0.20
0.15
0.10
0.05
0
PAX6
POU2F1
GATA5
PKM
DNMT3B
KIF21B
miR-E SCR
IgG
miR-E USP7 #A
IgG
miR-E USP7 #B
IgG

Fig EV3

A

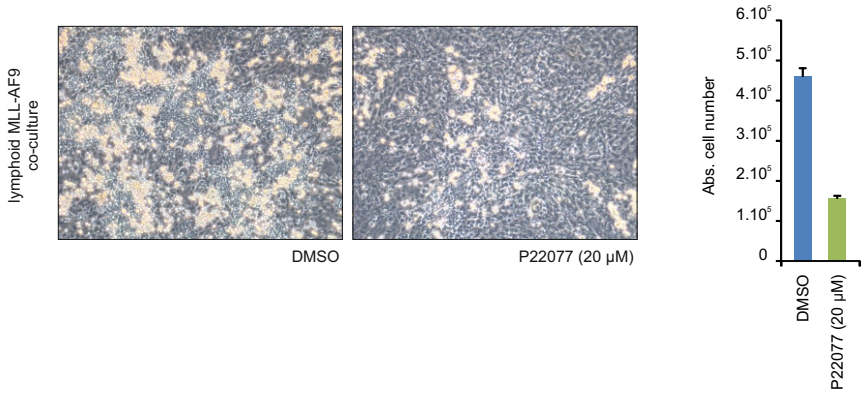
lymphoid MLL-AF9 co-culture
DMSO
P22077 (20 µM)
Abs. cell number
6.10^5
5.10^5
4.10^5
3.10^5
2.10^5
1.10^5
0
DMSO
P22077 (20 µM)